CNRS
Centre National de la Recherche Scientifique

INFN
Istituto Nazionale di Fisica Nucleare

Advanced Virgo Injection Mode-Matching Telescope Mechanics

VIR-0584A-13

Johannes Amarni, Jean-Pierre Baronick, Matteo Barsuglia,
Walter Bertoli, Christelle Buy, Alberto Gatto, Matteo Tacca

Issue: 2

Date: August 6, 2014

VIRGO * A joint CNRS-INFN Project
Via E. Amaldi, I-56021 S. Stefano a Macerata - Cascina (Pisa)
Secretariat: Telephone (39) 050 752 521 * FAX (39) 050 752 550 * Email W3@virgo.infn.it

Contents

1 Introduction

This document describes the mechanical mounts that hold the optical components of the Advanced Virgo Injection Mode Matching Telescope (MMT). After a short description of the telescope design, the mechanical parts realized at the Laboratoire AstroParticule et Cosmologie (APC) are described - plans are in attached files - and the validation tests are presented.

2 Mode Matching Telescope Design

The complete description of the Advanced Virgo Injection Mode Matching Telescope is provided in [1, 2]. In this document, the optical configuration and the telescope requirements are shortly summarized.

2.1 Optical configuration

The MMT, installed on the Suspended Injection Bench, is a catadioptric telescope composed by two parabolic mirrors and one meniscus diverging lens[1]. The layout is presented in figure 1. The great advantage of this configuration is its compactness which is mandatory because of space constraints on the bench. The two parabolic mirrors form an afocal off-axis parabolic telescope which increases the beam size by a factor 8.5 (i.e. from 2.6 mm to 22 mm). The diverging lens is used in combination with the Power Recycling mirror to further enlarge the beam size and match it to the interferometer.

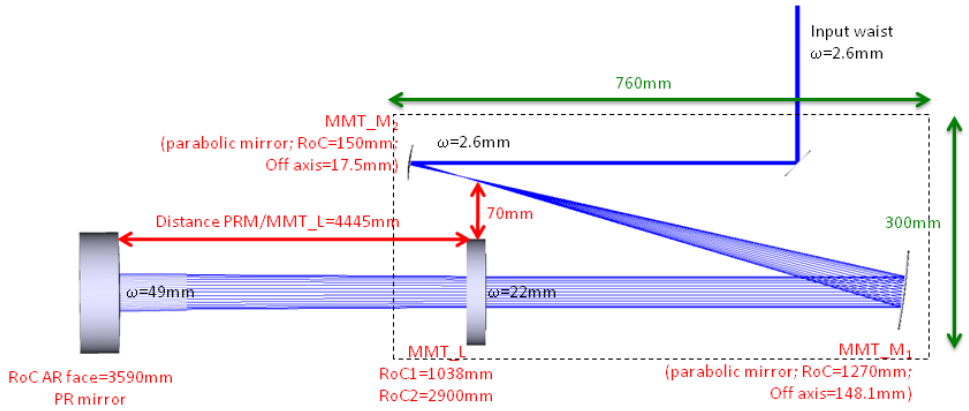

Figure 1: Advanced Virgo Input Mode Matching Telescope layout.

2.2 General requirements

The main requirements of the Injection MMT are given in the table 1. Considering manufacturing errors on optical elements parameters and alignment errors, the telescope should have the capacity to recover a matching with the interferometer higher than 99 %.

2.2.1 Requirements on the displacement ranges of the optical elements

Requirements on the displacement range of the optical elements of the telescope have been computed using a Monte Carlo simulation (Zemax^{TM} software). We have considered errors on the surface of the optics - radii of

[1]The Power Recycling Mirror is the fourth element of the telescope.

Parameter	Requirement
Mode matching on the ITF	$\geq 99\%$
Noise coming from diffused and back-reflected light	$\leq$ AdV sensitivity / 10
Telescope dimensions	$\leq$ 800 mm x 350 mm

Table 1: Injection Mode Matching Telescope requirements.

curvature (RoCs) and surface irregularities - and errors on the input beam parameters. All the details of the study are described in [1]. In this document only the main results are summarized because they have driven the design of the mechanical mounts and their motorizations.

• Radius of curvature errors

Errors in the RoCs set limits on the translation ranges. The potential error on the RoCs of the telescope optics considered here is 1%, which is an usual value given by manufacturers. In order to compensate for these errors and recover an optimal matching ($> 99\%$) on the interferometer 2 *compensators* can be - alternatively - used: the distance between the two parabolic mirrors and the distance between the meniscus lens and the PR mirror. Results are summarized in table 2.

Optical Element	**RoC Value (mm)**	**MMT_M1 / MMT_M2 (mm)**	**PR_AR / MMT_L (mm)**
MMT_M1	1270 ± 13	± 6	± 150
MMT_M2	90 ± 1.5	± 0.8	± 25
MMT_L face 1	1038 ± 11	± 2	± 50
MMT_L face 2	2900 ± 29	± 0.7	± 21
PR_AR	3590 ± 36	± 3	± 81

Table 2: Tolerancing results of the study: RoC values with errors and correspondent ranges of the compensators.

• Input beam errors

The input beam coming from the Faraday isolator and impacting on the telescope could present errors on the waist size or the waist position. If we consider - reasonable - errors on the beam waist size of 4 % and errors on the beam waist position of 500 mm, it is possible to recover a matching higher than 99 % by changing the distance between the PR mirror and the meniscus lens less than 1 mm.

• Surface irregularities

Typically the manufacturers give an accuracy on the Peak-to-Valley (PtV) surface irregularities of the order of $\lambda/5$ and an rms of $\lambda/50$. To compensate for these errors and recover a matching higher than 99 %, the distance between the two parabolic mirrors should be adjusted by +/- 0.6 mm or the distance between the meniscus lens and the PR mirror by +/- 15 mm.

2.2.2 Requirements on the motorization of the degrees of freedom

A tilt or a miscentering of the optics of the telescope induce coma and spherical aberrations. The Monte Carlo simulation has been run considering errors in the alignment of the optics. The maximum tilt and miscentering allowed to keep a matching higher than 99 % during the alignment phase are presented in table 3. The motorization should allow a minimum incremental motion much lower - a factor 10 - than the values in table 3.

A first alignment of the mounts will be done by hands with a precision of few - 2 or 3 - millimeters. Then, motorizations will be used in order to meet the requirements and have reproducible motions. Actuators have to be compatible in a vacuum level of 10^{-6} mbar. The most critical degree of freedom is the alignment between the two parabolic mirrors MMT_M1 and MMT_M2. Therefore, closed-loop actuators are used. The transversal position of MMT_M2 is less critical and two open-loop actuators are used to center the laser beam. Moreover,

Defect	MMT_M1	MMT_M2	MMT_L
Tilt	300 μrad	425 μrad	17 mrad
Miscentering	100 μm	100 μm	100 μm

Table 3: Maximum tilt and miscentering allowed for the optics of the catadioptric telescope during alignment phase.

the laser beam is centered on MMT_M1 by the angular movements of MMT_M2, therefore the control of its transversal motions is not necessary. For what concern the meniscus lens, it is important to center it in order to avoid the introduction of aberration, but its alignment is less critical. Therefore, three open loop actuators are used for its transversal and longitudinal degrees of freedom.

2.2.3 Requirements on the stability of the mounts

Once the telescope is aligned, the maximum tilt and miscentering allowed on the optics in a stable phase (during science mode) have been computed in order to define requirements on the angular and transversal stability of the mounts. Results are presented in table 4, setting the requirements for the design of the mechanical mounts.

Defect	MMT_M1	MMT_M2	MMT_L
Tilt	0.84 μrad	6.8 μrad	1 mrad
Miscentering	100 μm	10 μm	100 μm

Table 4: Maximum tilt and miscentering allowed for the optics of the catadioptric telescope during science mode.

2.2.4 Requirements on the weight of the telescope

The weight of the Suspended Injection Bench + opto-mechanical parts has been estimated to 160 kg. This estimation has driven the design of the Super-Attenuator (filters). The MMT isn't the only part on the bench, it has to be lower than 20 kg in order to respect the estimation and meet the requirements.

2.2.5 Requirements on the resonance frequencies: diffused light noise projection

The projection of the diffused light noise by the MMT compared to the AdV sensitivity is shown in figure 2 [6], where the displacement of the mounts is considered equal to the displacement of the bench. In reality the displacement is amplified by the resonances of the mounts. This set a requirement on the resonance frequencies and the quality factor of the mounts: the noise coming from diffused and back-reflected light should be a factor 10 lower than the Advanced Virgo sensitivity.

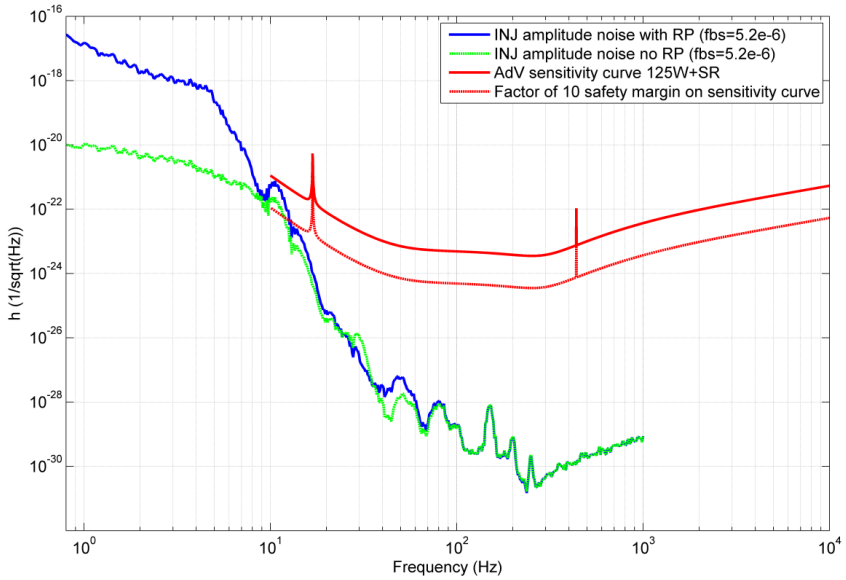

Figure 2: Scattered light noise projection: direct reflection of the second face of the meniscus lens.

3 Mechanical Mounts Description

In the following paragraph the properties of the mechanical mounts and the requirements in terms of movements are described. The three mounts are realized in aluminum alloy (AU4G) in order to satisfy the requirements on maximum weight and vacuum working condition (pressure of $\sim 10^{-6}$ mbar). A rotation system using gimbal joints is used to increase the rigidity of these two mounts and also to decouple the two axis of rotation. On MMT_M1 and MMT_M2, one of the parts - the gimbal joints - will be made of drawn bronze (UE9P) and aluminum alloy to allow the rotation of the mount around the joints without friction.

The motions of the three mounts are provided by a system made of picomotors, rails and springs. The main properties of the open loop picomotors, model 8301-UHV and 8303-V provided by Newport^{TM}, are summarized in table 5 (maximum speed, axial load capacity, maximum torque, ...). These picomotors will be installed on the MMT_L meniscus lens and MMT_M2 parabolic mirror. The properties of the closed loop picomotors, model 8310-V provided by Newport^{TM}, installed on MMT_M1 and MMT_M2 parabolic mirrors, are detailed in table 6.

The rails, which allow the guided motion along the three directions, are provided by Axmo Precision^{TM}. Crossed roller rails have been chosen because they are compact, they can support and guide high loads with high accuracy, repeatability, low friction and they are characterized by a quite high rigidity.

The springs have to produce a force in the opposite direction with respect to the one induces by the picomotors. They have been chosen to be such that their force is lower than the maximum load capacity of the picomotors, which is 22 N, (to allow the picomotors to move) but higher than frictional forces and keep the picomotors in contact with the mount. The characteristics of the springs used for the MMT_L meniscus lens, MMT_M1 and MMT_M2 parabolic mirrors are summarized in tables 7, 8 and 9.

The installation of two baffles is foreseen on the back of the two parabolic mirrors in order to dump the possible transmitted light.

For all the mounts "fake" optical elements in aluminum, characterized by the same weight and center of mass of the real elements, are produced to perform the mechanical tests.

Model	**8301-UHV**	**8303-V**
Travel Range	12.7 mm	50.8 mm
Minimum Incremental Motion	< 30 nm	< 30 nm
Maximum Speed	1.2 mm/min @ 2 kHz pulse rate	1.2 mm/min @ 2 kHz pulse rate
Axial Load Capacity	22 N	22 N
Maximum Torque	0.018 Nm	0.018 Nm
Vacuum Compatibility	10^{-9} Torr	10^{-6} Torr

Table 5: Properties of the picomotors installed on the meniscus lens and parabolic mirror M2 mounts.

Model	**8310-V**
Travel Range	12.7 mm
Minimum Incremental Motion	< 30 nm
Load Capacity	22 N
Mounting	0.375 in. shank

Table 6: Properties of the picomotors installed on the parabolic mirrors M1 and M2 mounts.

	x	**y**	**z**
Stiffness (daN/mm)	0.0562	0.0654	0.0138
Length (mm)	15.7	15.7	45.1
Diameter (mm)	6.2	7.2	9.5

Table 7: Properties of the springs installed on the meniscus lens mount.

	pitch	**yaw**	**z**
Stiffness (daN/mm)	0.0654	0.0654	0.0654
Length (mm)	15.7	15.7	15.7
Diameter (mm)	7.2	7.2	7.2

Table 8: Properties of the springs installed on the parabolic mirror M1 mount.

	pitch	**yaw**	**x**	**y**
Stiffness (daN/mm)	0.0562	0.0562	0.0654	0.0562
Length (mm)	15.7	15.7	15.7	15.7
Diameter (mm)	6.2	6.2	7.2	6.2

Table 9: Properties of the springs installed on the parabolic mirror M2 mount.

3.1 Meniscus Lens MMT_L Mount

This mount has to hold a meniscus lens with a diameter of 150 mm and a thickness of 25 mm. The total weight, including the lens, is 5.1 kg. Following 2.2.4, the MMT_L mount has to allow translations along the three orthogonal directions (x, y, z)[2]. Figure 3 shows a view of the 3D design of the mount.

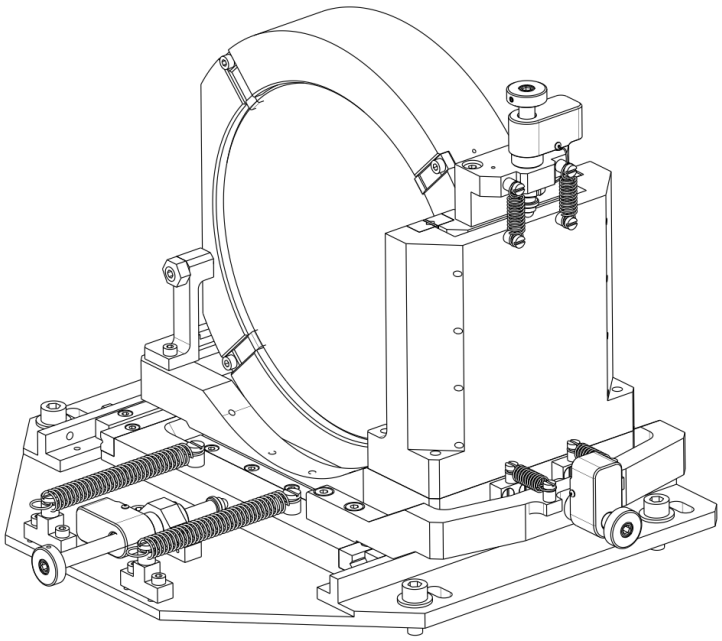

Figure 3: Meniscus lens MMT_L mount design.

The picomotors are 8301-UHV for the movements along x and y and 8303-V for the motion along z. The ranges in the three directions provided by the picomotors are $\Delta x = \Delta y = \pm$ 6 mm and $\Delta z = \pm$ 25 mm. The distance between the PR mirror and the meniscus lens could vary in a range of ±150 mm (2), which is larger than the travel range of the picomotors (± 25 mm). Therefore, the meniscus lens will be pre-aligned by hand with a precision of few millimeters and only the final tuning will be made by the picomotor, as explained in the paragraph 2.3.

Moreover, the minimum incremental motion of the picomotors (30 nm as explained in table 5) satisfy the requirements for the alignment of the telescope, as described in 2.2.4.

Figure 4 shows two pictures of the meniscus lens mount realized at the APC.

[2]x and y are defined as the horizontal and the vertical axes orthogonal to the beam propagation and z as the axis parallel to the beams propagation and, therefore, parallel to the axis of the lens.

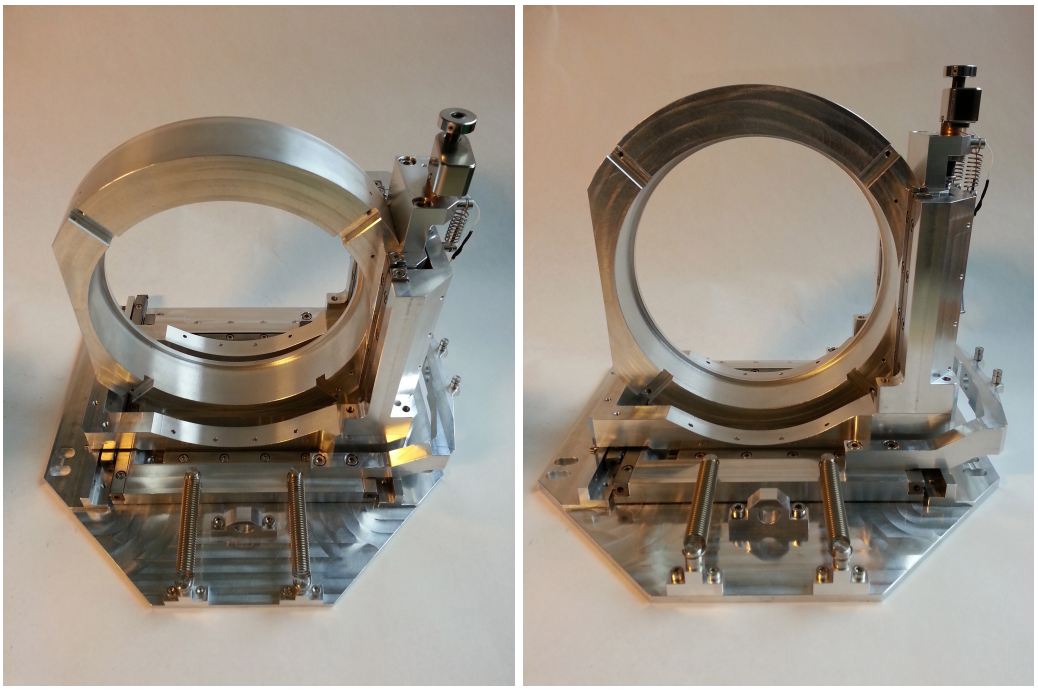

Figure 4: Meniscus lens mount.

3.2 Parabolic Mirror MMT_M1 Mount

This mount has to hold a parabolic mirror with a diameter of 150 mm and a thickness that varies between 15 mm (thin side) and 32 mm (thick side). Its total weight, including the mirror, is about 4.20 kg. It has to allow movements along one longitudinal (z) and two angular (pitch and yaw) directions. Figure 5 shows one view of the 3D design of the mount.

The used picomotors are all closed loop 8310-V. The ranges of the movements are respectively $\Delta\theta_x = \Delta\theta_y = \pm 85$ mrad and $\Delta z = \pm$ 6 mm. They meet the requirements summarized in tables 2 and 3 to align the mirror.

Figure 6 shows two pictures of the parabolic mirror M1 mount realized at the APC.

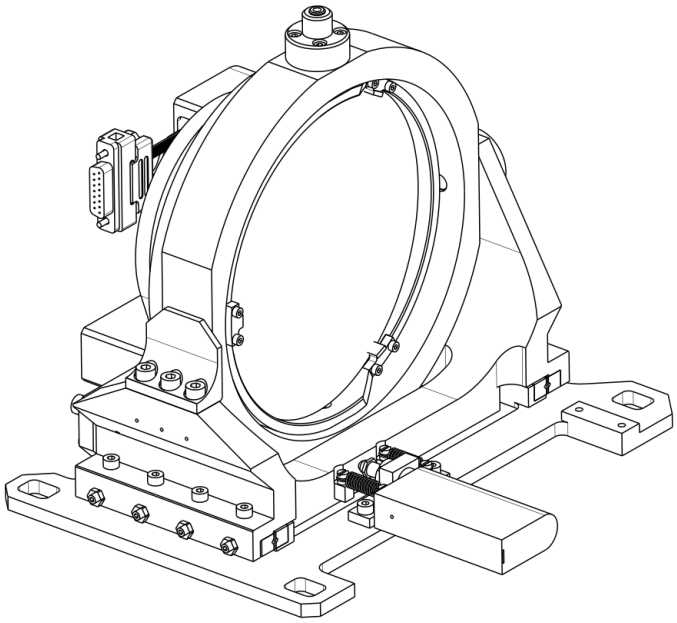

Figure 5: Parabolic mirror MMT_M1 mount design.

Figure 6: Parabolic mirror MMT_M1 mount.

3.3 Parabolic Mirror MMT_M2 Mount

This mount has to hold a parabolic mirror with a diameter of 30 mm and a thickness that varies between 8 mm (thin side) and 14 mm (thick side). Its total weight, including the mirror, is about 2.4 kg. The mount has to allow movements along two transversal (x,y) and two angular (pitch and yaw) directions. Figure 7 shows one view of the 3D design of the mount.

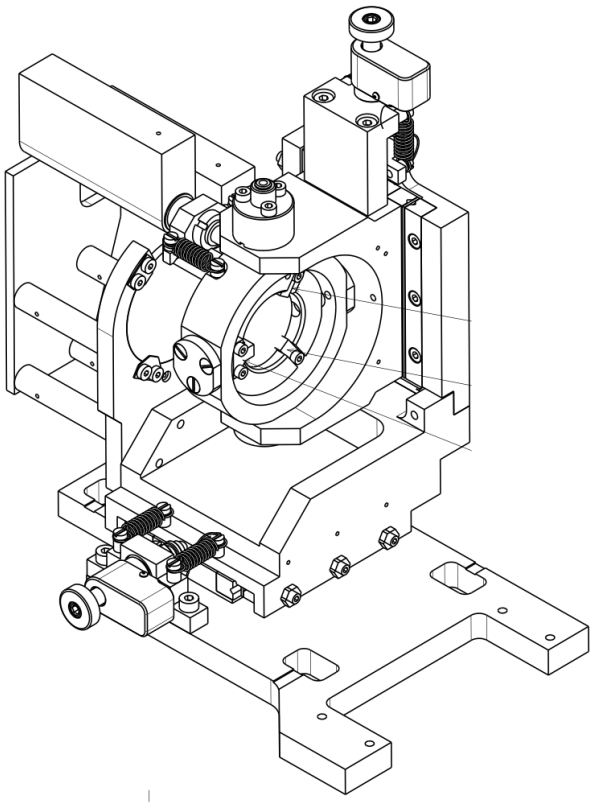

Figure 7: Parabolic mirror MMT_M2 mount design.

The two picomotors used for the angular movements are 8310-V, whereas the two ones used for the longitudinal motions are 8301-UHV. The ranges of the movements provided by the picomotors are respectively $\Delta\theta_x = \Delta\theta_y = \pm$ 420 mrad and $\Delta x = \Delta y = \pm$ 6 mm, which meet the requirements summarized in tables 2 to align the mirror.

Figure 8 shows a picture of the parabolic mirror M2 mount realized at the APC.

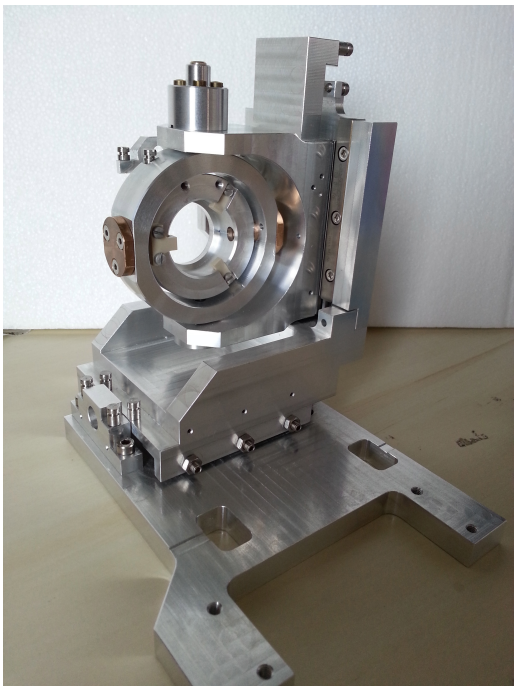

Figure 8: Parabolic mirror MMT_M2 mount.

4 Mechanical Tests

In order to validate the mechanical mounts the following tests have been performed:

- characterization of the displacements (translation and rotation);
- short term and long term stability;
- measurement of the resonance frequencies and quality factors.

Tests have been performed both in-air and in-vacuum in order to study the behavior of the mounts in its final working condition. A mechanical comparator and a system of two optical levers have been used to check the movements and the stability. In order to measure the resonance frequencies of the mounts, an electromagnetic excitation has been used.

4.1 Characterization of translations and tilts

In order to check the right functioning of the mounts, movements in the various degrees of freedom are induced by picomotors. During the experimental tests, only open loop picomotors - model 8301 - (whose absolute position is not precisely known) have been installed[3]. All the mounts movements are measured using both a mechanical comparator and an optical levers setup. Measurements are performed both in air and under vacuum.

4.1.1 Optical levers system

In order to measure the movements of the mounts and possible couplings among the different degrees of freedom a system of two optical levers is used. Considering a system composed by one converging lens with a focal length

[3]For clearness reason and spare number of closed loop picomotors, the Injection Subsystem decided that all the tests will be performed using open loop picomotors, even for MMT_M1 and MMT_M2.

f, the longitudinal displacement x_2 and the angular displacement θ_2 at the output of the system as a function of the longitudinal displacement x_1 and of the angular displacement θ_1 can be described as:

$$\begin{bmatrix} x_2 \\ \theta_2 \end{bmatrix} = \begin{bmatrix} 1 & d_2 \\ 0 & 1 \end{bmatrix} \begin{bmatrix} 1 & 0 \\ -1/f & 1 \end{bmatrix} \begin{bmatrix} 1 & d_1 \\ 0 & 1 \end{bmatrix} \begin{bmatrix} x_1 \\ \theta_1 \end{bmatrix} \tag{4.1}$$

where d_1 and d_2 are the distances between the lens and respectively the input and the output of the system. Therefore, the longitudinal displacement at the output of the system x_2 is expressed as:

$$x_2 = \left(1 - \frac{d_2}{f}\right) x_1 + \left(d_1 + d_2 - \frac{d_1 d_2}{f}\right) \theta_1 \tag{4.2}$$

From equation 4.2 it could be seen that the quadrant sensible only to the angular displacements should be installed in the focal plane of the system (Far Field Quadrant, FFQ), whereas the quadrant sensible only to the longitudinal movements should be placed in the image plane (Near Field Quadrant, NFQ).

A scheme and a picture of the implemented system are shown in figure 9.

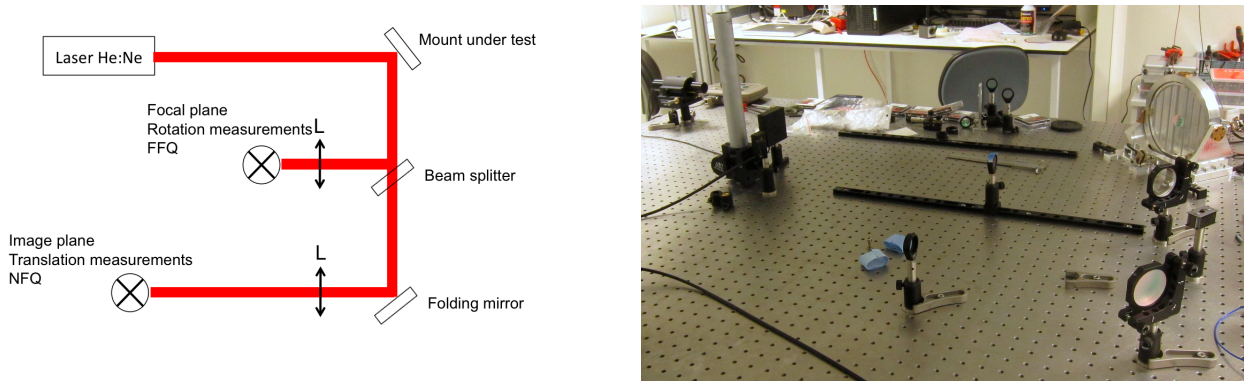

Figure 9: Optical levers setup.

A He-Ne laser (model HNL008L-EC by Thorlabs^{TM}) is used as source of the input beam (output power $P = 0.8$ mW, beam diameter $d = 0.48$ mm, divergence $\theta\infty = 1.7$ mrad). After impinging on a mirror held by the mount under tests, the laser beam is divided by a beam splitter and is sent separately to the Near Field and the Far Field quadrants. In both the optical levers a converging lens with a focal length of $f = 500$ mm is installed. Two quadrant photodiodes of the model PDQ80A by Thorlabs^{TM} are used. They are characterized by a peak responsivity of 0.4 A / W at 633 nm, a transimpedance gain of 10 kV / A, a bandwidth of 150 kHz and a sensing area of a diameter of 7.8 mm.

The calibration of the system has been made, first by calibrating the picomotors and then by calibrating the quadrant photodiodes.

• Calibration of the picomotors

In order to measure a calibration coefficient between steps of the picomotors and radians for the angular movements of the mounts, a folding mirror has been add on the optical system, just after the mount under test, in order to send the beam on a screen at a distance of ~ 2 m. Large movements of the mounts have been realized in the angular degrees of freedom to visualize macroscopic displacement of the beam on the screen. By measuring the distance between the mount and the wall it is easy to calculate the calibration coefficient between steps of the picomotors and radians displacements of the mount. In order to measure a calibration coefficient between steps of the picomotors and meters, a mechanical comparator is used. Large movements of the mounts have

been induced in the longitudinal directions and the effective motions have been measured by the comparator calculating easily the calibration coefficient between steps of the picomotors and meters. The results for each mechanical mounts are summarized in tables 10, 11 and 12. Note that the incremental motion of the picomotor quoted by the manufacturer is 30 nm. Since the picomotor is open loop the maximum angular motion for 1 step is 4.10^{-7} rad for M1 and 2.10^{-6} for M2, but it can be lower. Moreover, the maximum transversal motion for 1 step should be 3.10^{-8} m for the three mounts. This is in agreement with the measurements obtained and presented in the following tables.

	NFQ_x	**NFQ_y**	**NFQ_z**
rad / steps	-	-	-
m / steps	2.10^{-8}	2.10^{-8}	2.10^{-8}

Table 10: Calibration coefficients measured for the MMT_L mount.

	FFQ_pitch	**FFQ_yaw**	**NFQ_z**
rad / steps	3.10^{-7}	2.10^{-7}	-
m / steps	-	-	2.10^{-8}

Table 11: Calibration coefficients measured for the MMT_M1 mount.

	FFQ_pitch	**FFQ_yaw**	**NFQ_x**	**NFQ_y**
rad / steps	3.10^{-7}	2.10^{-7}	-	-
m / steps	-	-	2.10^{-8}	2.10^{-8}

Table 12: Calibration coefficients measured for the MMT_M2 mount.

• Calibration of the quadrant photodiodes

At first, the linearity of the response of the quadrant has been checked in order to define the working range. Starting from the center of the sensor, some measurements have been made up to the end of the sensible area. Figure 10 shows an example of the obtained results. The response of the quadrant is linear up to an output voltage of ~ 0.65 V.

In order to obtain calibration coefficients in rad / V and m / V small calibrated displacements of the parabolic mirror M1 mount have been made to measure the angular and transversal motions of the beam in the plane of the quadrants. According to the tables 10, 11, 12 and considering the motions of the mounts calibration coefficients for each quadrant photodiodes are calculated: for the Far Field quadrant the obtained coefficient is 3.10^{-4} rad / V, for the Near Field quadrant it is 3.10^{-4} m / V.

Note that these measurements have been made with an incertitude of the order of 10%, related to the measure of the displacements on the screen (for the calibration of the picomotors) or the measure on the plane of the quadrants (for the calibration of the quadrants).

Finally, an upper limit of the coupling between the two direction of each quadrants (Horizontal and Vertical) and an upper limit of the coupling between the two quadrant photodiodes (FFQ and NFQ) have been found in order to have the sensing matrix of the whole system (signals of the quadrant photodiodes are expressed in V, angular movements in rad and displacements in m).

$$\begin{bmatrix} FFQ_V \\ FFQ_H \\ NFQ_H \\ NFQ_V \end{bmatrix} = 3.3 * 10^3 \begin{bmatrix} 1 & 0.05 & 0.03 & 0.03 \\ 0.05 & 1 & 0.03 & 0.03 \\ 0.03 & 0.03 & 1 & 0.05 \\ 0.03 & 0.03 & 0.05 & 1 \end{bmatrix} \begin{bmatrix} \theta_x \\ \theta_y \\ x \\ y \end{bmatrix} \tag{4.3}$$

Therefore, the upper limit of the coupling introduced between the two directions of each quadrant is 5 % and the one of the coupling between the two quadrant photodiodes is 3 %.

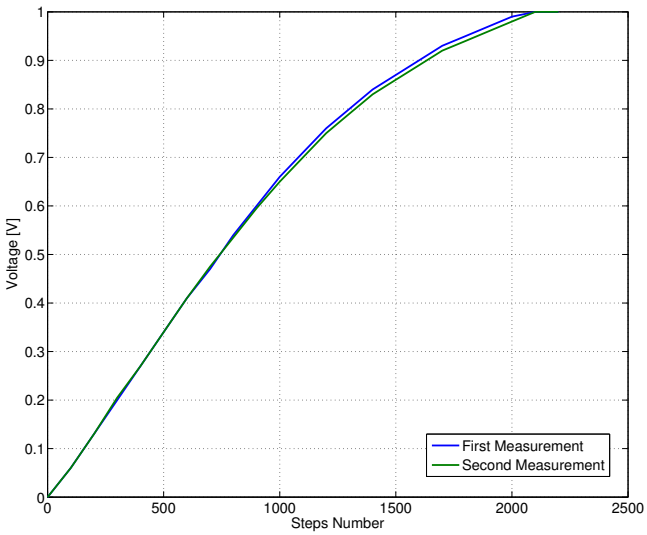

Figure 10: Measured response of the quadrant photodiode used in the tests.

4.1.2 In vacuum system

In order to make a characterization of the mechanical mount in vacuum, a cylindrical vacuum tank, characterized by a diameter of 50 cm and a height of 30 cm, is used (figure 11).

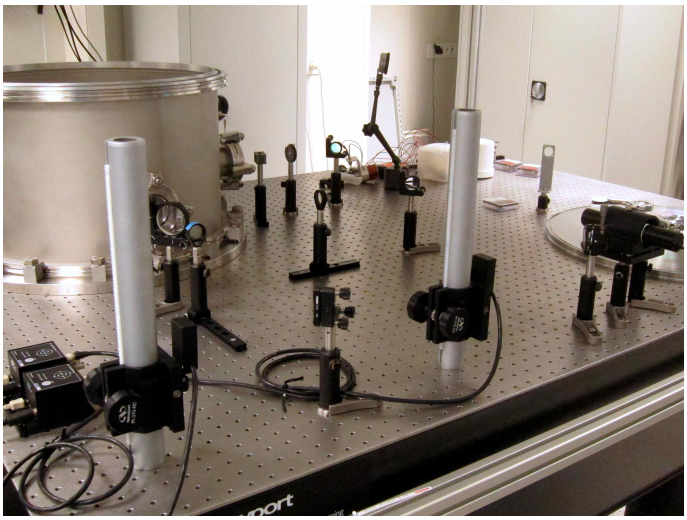

Figure 11: Optical setup and vacuum tank.

Figure 12 shows the picture of the mechanical mount under test installed inside the vacuum tank together with the coil system used for the electromagnetic excitation.

The typical trend of the pressure inside the tank is shown in figure 13.

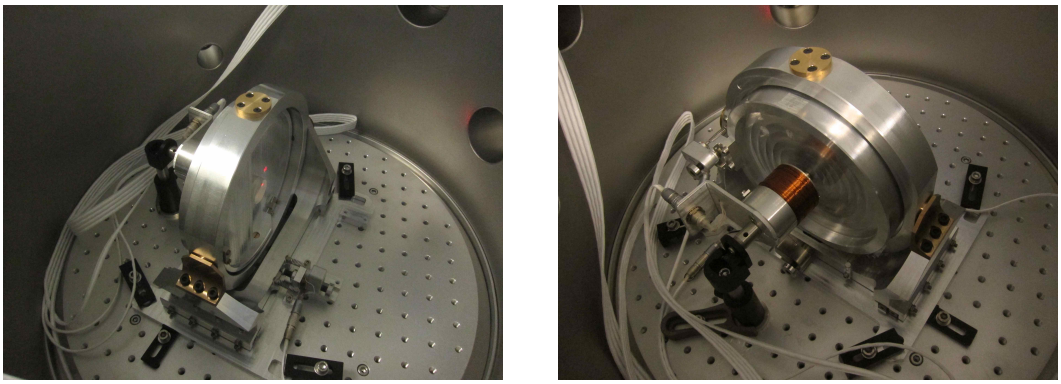

Figure 12: Parabolic mirror M1 mount installed inside the vacuum tank.

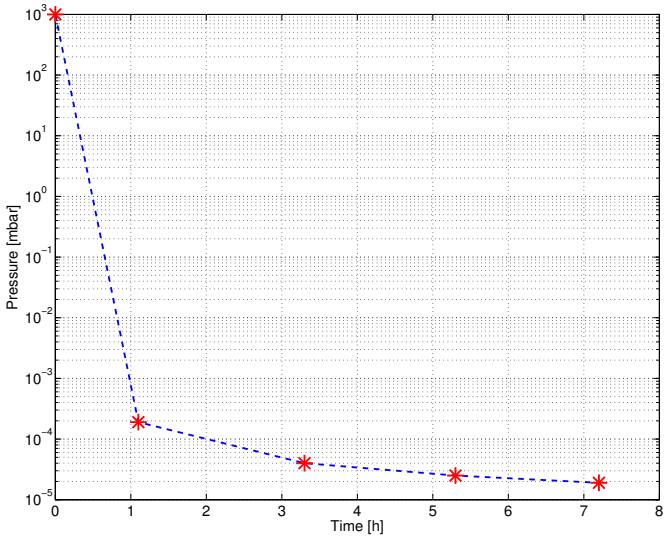

Figure 13: Pressure trend inside the vacuum tank.

4.1.3 Characterization of the motions of the MMT_L Mount

The movements in the three translations (x, y, z) of the meniscus lens mount are first tested with a mechanical comparator (see picture 14). For every test, the motion is induced in a single direction by the corresponding picomotor. Tests for motions of different lengths have been performed (from 0.04 mm to 0.6 mm): in all the measurements the mechanical mount in both directions (forward and backward) moved of the expected quantity, confirming the good functioning of the system made of rails, springs and picomotors.

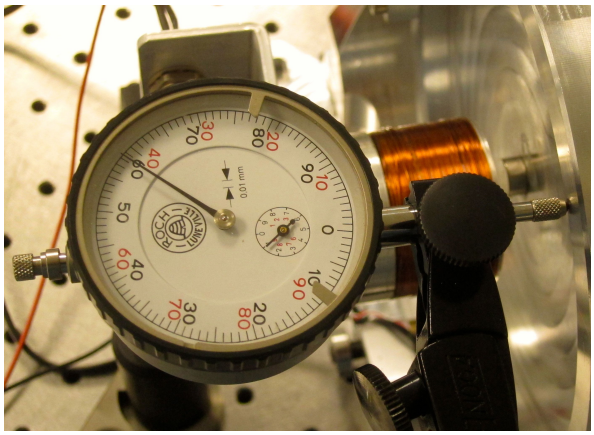

Figure 14: Mechanical comparator used for measurements of the movements of the mounts.

Moreover, motions are tested also with the optical levers. In particular, movements along z produce displacements that are detectable by the horizontal direction of the quadrant. The behavior in air and in vacuum was the same and, as an example of the obtained results, the displacement measured in air is shown in figure 15.

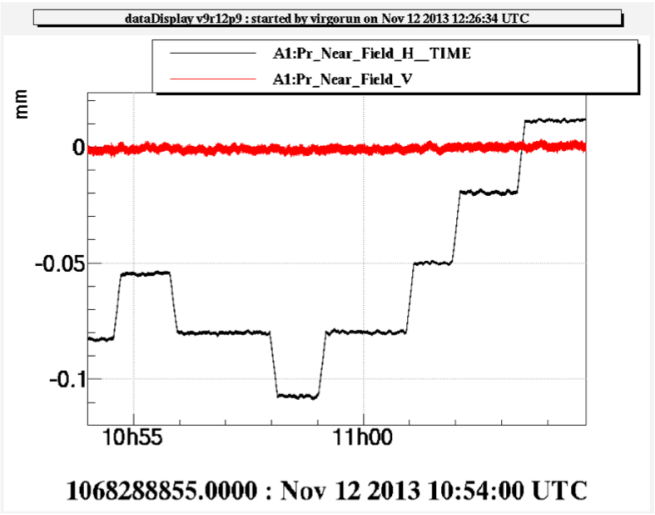

Figure 15: Test of the transversal of the meniscus lens mount in z direction in air.

In order to check that the mount correctly moves in x and y another method has been used: a tilted plane mirror is glued on the fake lens held by the mount. In this configuration motions can be detected by the quadrants. The tilt imposed to the mirror cannot be very large due to the geometrical constraints of the setup and cannot be measured. The signals on the quadrants are not calibrated and we can only check that the measurements is repeatable. Obtained results are shown in figure 16 and 17 for motions induced on the mount respectively in x and y directions.

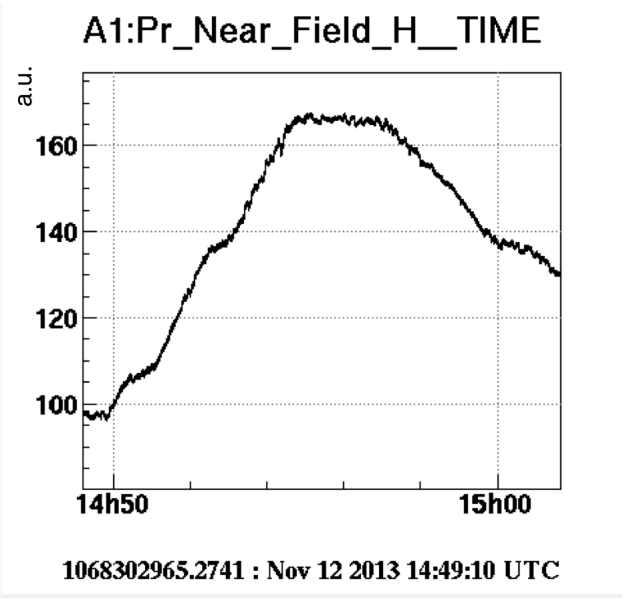

Figure 16: Test of the transversal motion of the meniscus lens mount in x direction. In this configuration the fake mirror is slightly tilted by an unknown amount in order to make the setup sensitive to transversal direction. For this reason the calibration is not known and the motion is indicated in arbitrary units.

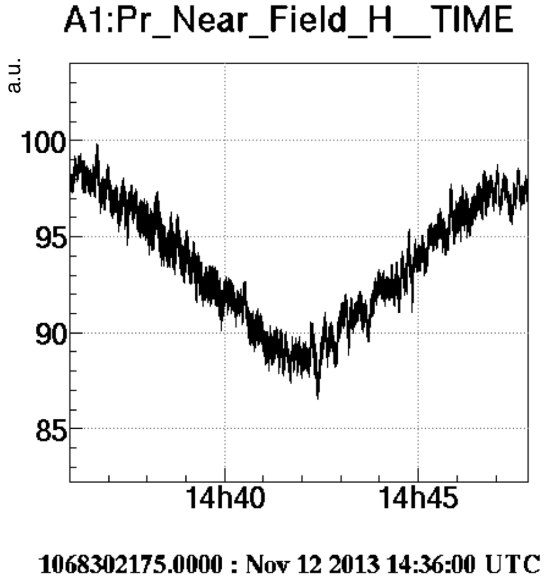

Figure 17: Test of the transversal motion of the meniscus lens mount in y direction. In this configuration the fake mirror is slightly tilted by an unknown amount in order to make the setup sensitive to transversal direction. For this reason the calibration is not known and the motion is indicated in arbitrary units.

In conclusion, the MMT_L mount moves correctly in the three (x, y, z) degrees of freedom and the behaviour is the same in air and under vacuum. Several measurements have been made and the movements are repeatable. The coupling between z and other degrees of freedom (x and y) is less than 5 %, the same order of the system sensing noise.

4.1.4 Characterization of the motions of the MMT_M1 Mount

Figure 18 shows a motion of the mount in the yaw direction and the corresponding motion in pitch measured with the Far Field quadrant when the corresponding picomotor is actuated. A tilt with an amplitude of 60 μrad is measured in yaw; while in pitch a motion less than 1 μrad is measured. The coupling between yaw and pitch is less than 2 %.

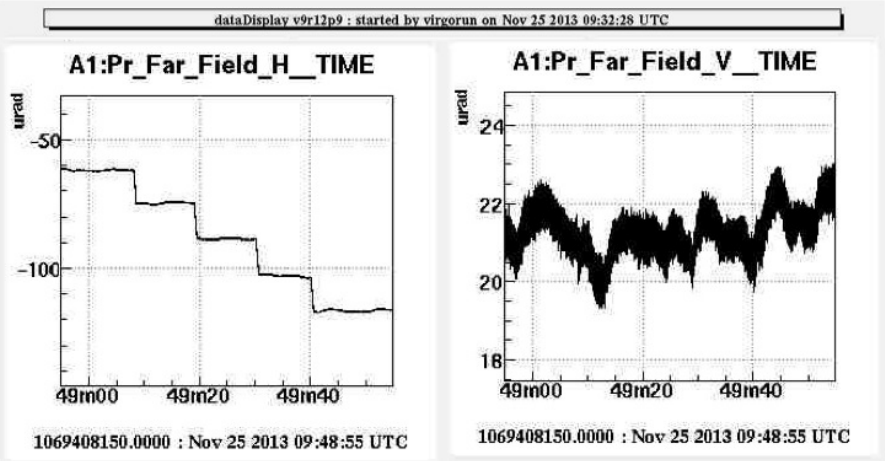

Figure 18: Motion in yaw of the M1 mount: (left) yaw signal and (right) pitch signal.

Figure 19 shows a motion of the mount in pitch direction and the corresponding motion in yaw measured with the Far Field quadrant when the corresponding picomotor is actuated. The pitch amplitude is 40 μrad and the yaw is 2 μrad. The coupling between pitch and yaw is 5 %.

Figure 20 we show a typical displacement measured by the Near Field quadrant for a motion of the mount along z.

In conclusion, the system of picomotors, rails and springs is working correctly on the MMT_M1 mount. It induces a right movement of the mount. The coupling between the angular degrees of freedom is less than 5 %, a value comparable with the coupling introduced by the sensing system; it is enough to align the telescope, also considering that the final mount will be controlled by closed loop picomotors.

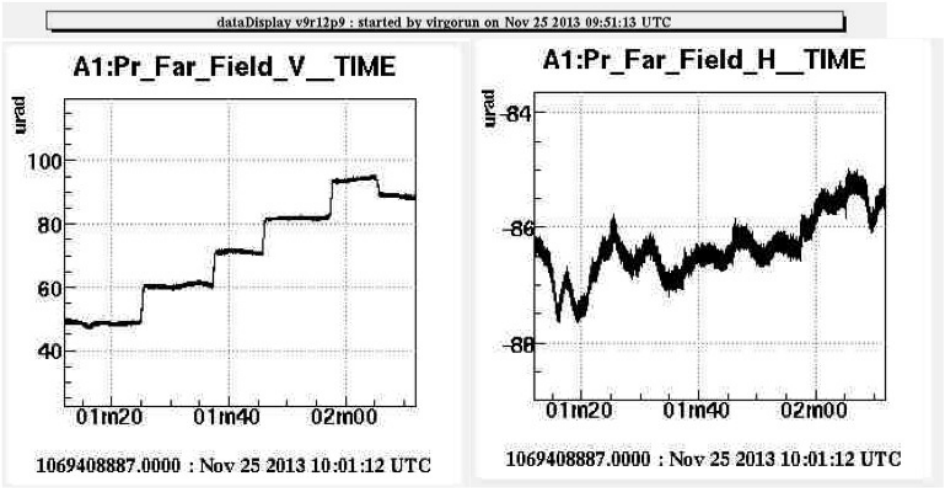

Figure 19: Motion in pitch of the M1 mount: (left) pitch signal and (right) yaw signal.

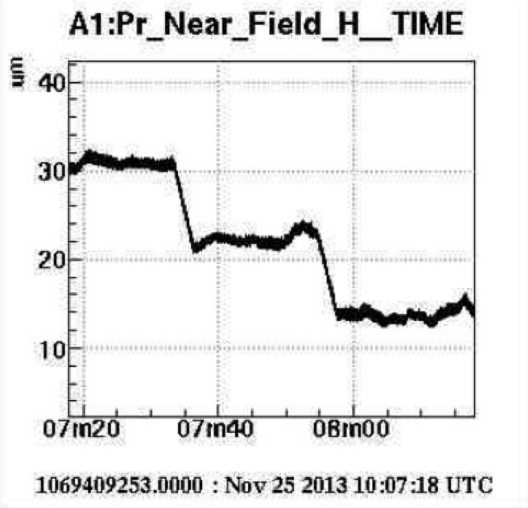

Figure 20: Test of the transversal motion of the M1 mount in z.

4.1.5 Characterization of the motions of the MMT_M2 Mount

Figure 21 shows a motion of the mount in the yaw direction and the corresponding motion in pitch measured with the Far Field quadrant when the corresponding picomotor is actuated. A tilt with an amplitude of 33 μrad is measured in yaw; while in pitch a motion less than 1 μrad is measured. The coupling between yaw and pitch is less than 3 %.

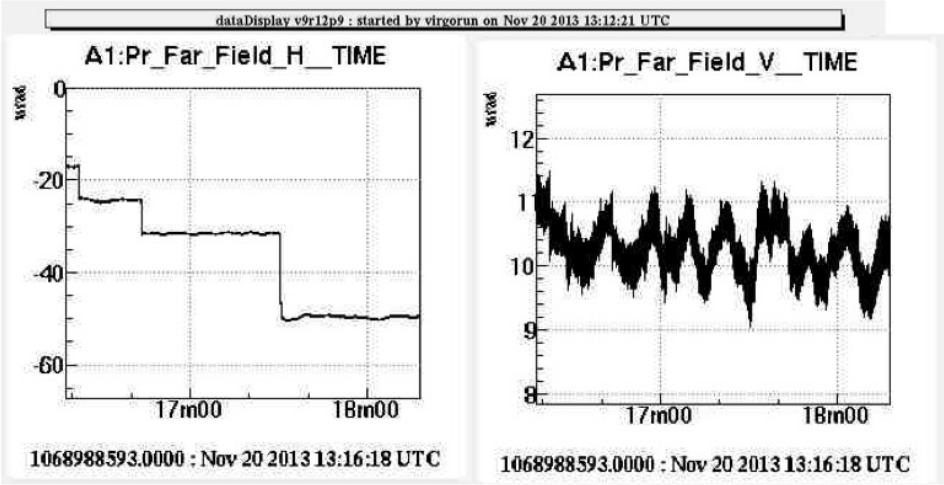

Figure 21: Motion in yaw of the M2 mount: (left) yaw signal and (right) pitch signal.

Since some backlash problems have been discovered, the MMT_M2 mount has been modified after the tests. More details are described in the Appendix A. Figure 22 shows the motions of the mount in the angular directions (black: yaw, red: pitch) measured with the Far Field quadrant: the mount can move in both directions with a coupling lower than 5 %. The peaks visible in yaw during the pitch movements are probably connected to the vibrations that the picomotor induces to the ball of the vertical axis (picomotor and ball are very close).

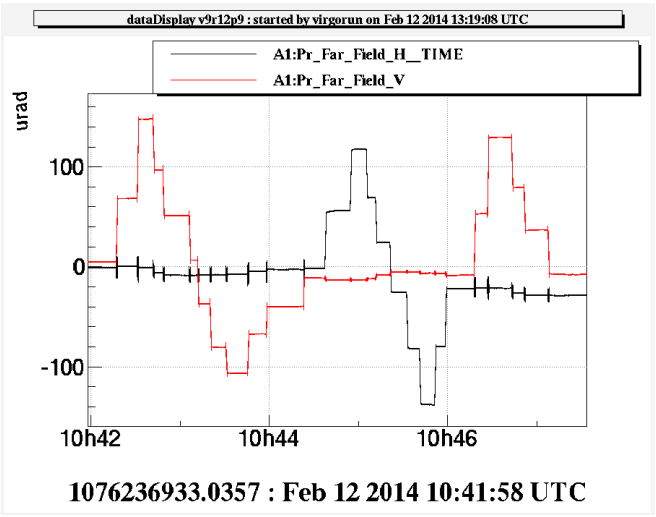

Figure 22: Angular motion of the M2 mount: (red) pitch signal and (black) yaw signal.

In order to check that the mount correctly moves in x and y, the plane mirror held by the mount has been tilted. In this configuration motions can be detected by the quadrants. The tilt imposed to the mirror cannot be very

large due to the geometrical constraints of the setup and cannot be measured. The signals on the quadrants are not calibrated and we can only check that the measurements is repeatable. Obtained results are shown in figure 23 and 24 for motions induced on the mount respectively in x and y directions.

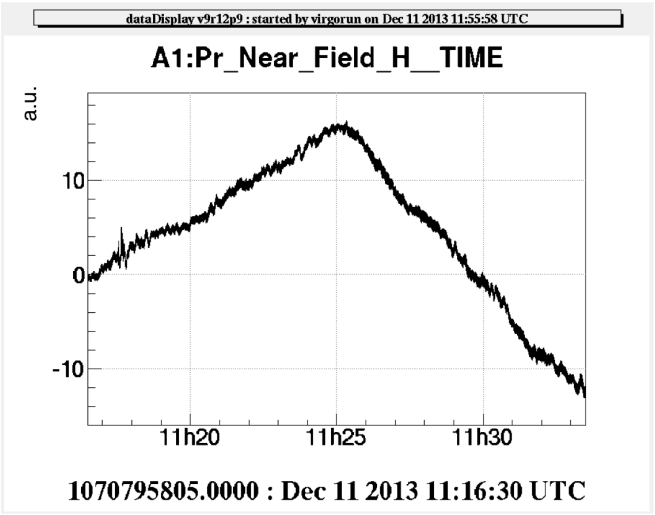

Figure 23: Test of the transversal motion of the M2 mount in x direction. In this configuration the fake mirror is slightly tilted by an unknown amount in order to make the setup sensitive to transversal direction. For this reason the calibration is not known and the motion is indicated in arbitrary units

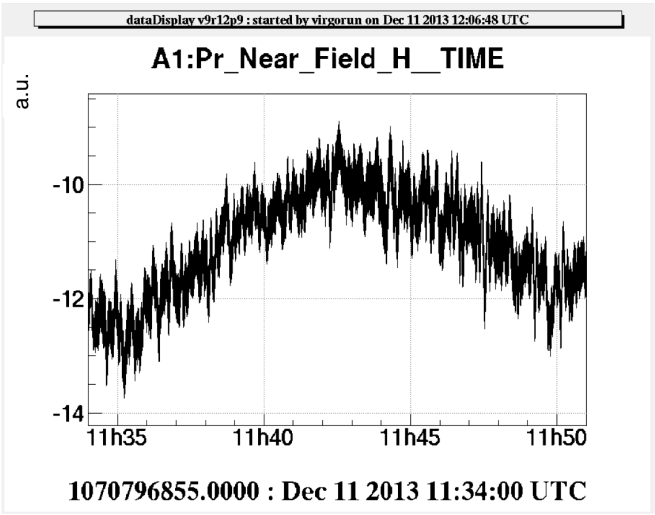

Figure 24: Test of the transversal motion of the M2 mount in y direction. In this configuration the fake mirror is slightly tilted by an unknown amount in order to make the setup sensitive to transversal direction. For this reason the calibration is not known and the motion is indicated in arbitrary units

In conclusion, the system of picomotors, rails and springs is working correctly on the MMT_M2 mount. It induces right movements of the mount. The coupling between the angular degrees of freedom is less than 6 %, a value comparable with the coupling introduced by the sensing system. Moreover, the mount will be controlled by two closed loop picomotors for the angular degrees of freedom, allowing to have an absolute reference.

4.2 Stability of the mechanical mounts

In order to detect any suspect anomalous glitch or drift of the mounts (that would be due to potential manufacturing defects), several short time and long time measurements have been done. These measurements have been compared to the noise and the drift of the setup.

4.2.1 Noise of the optical levers system

The noise of the setup has been measured replacing the telescope mount under test with a standard mount, similar to the other mounts of the setup (a post, a post holder and a mirror mount). Figure 25 shows the measured signals.

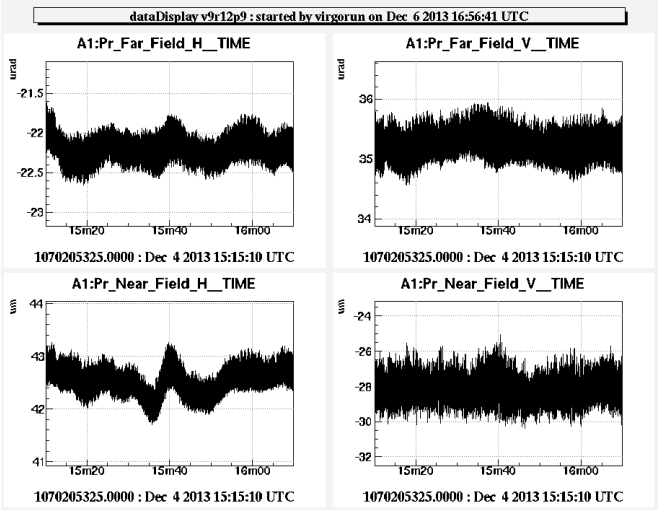

Figure 25: Typical noise of the experimental setup in the four degrees of freedom: top (left) yaw, (right) pitch; bottom (left) x, (right) y.

Results obtained for the rms values (on 60 s) are:

- equivalent pitch noise: ~ 0.2 μrad
- equivalent yaw noise: ~ 0.3 μrad
- equivalent x noise: ~ 0.3 μm
- equivalent y noise: ~ 0.6 μm

At the beginning of the experiment the main source of noise was due to air fluctuations and acoustic vibrations, caused by the clean air system of the room . In fact, all the long time measurements showed the same behavior: a small drift and many glitches. In order to solve this problem, the setup has been covers withs boxes. A comparison between results obtained for the horizontal direction of the near field quadrant in two different configurations of the setup - with and without boxes - is shown in figures 26 and 27. In particular, figure 26 shows a long time measurement (black curve: no protection boxes on the setup; purple curve: boxes on the setup) and figure 27 (black curve: boxes on the setup; purple curve: no boxes on the setup) shows a short time measurement: the level of the noise in the configuration with boxes and covers on the setup is much lower. All the results presented in this document are obtained with boxes and covers on the experimental setup.

Another important source of noise is the scattered light that can recombine with the optical beam. In particular, the main sources of scattered light and spurious beams are the two windows of the vacuum tank, the beamsplitter, which is installed just at the output of the vacuum tank divides the beam in the Near Field and Far Field

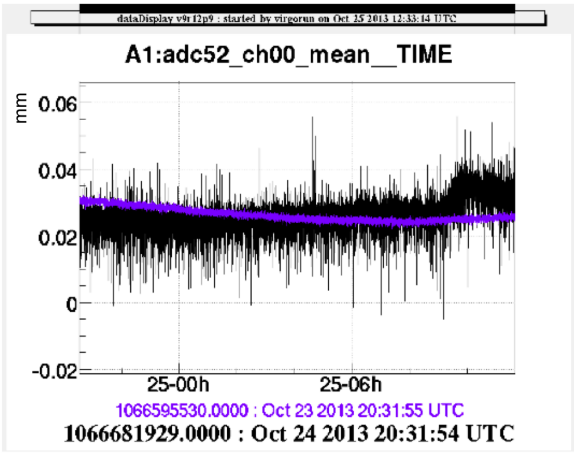

Figure 26: Near Field quadrant long time (16 hours) signal measured for a standard mount: comparison between the configuration with boxes and cover on the setup and configuration without protections.

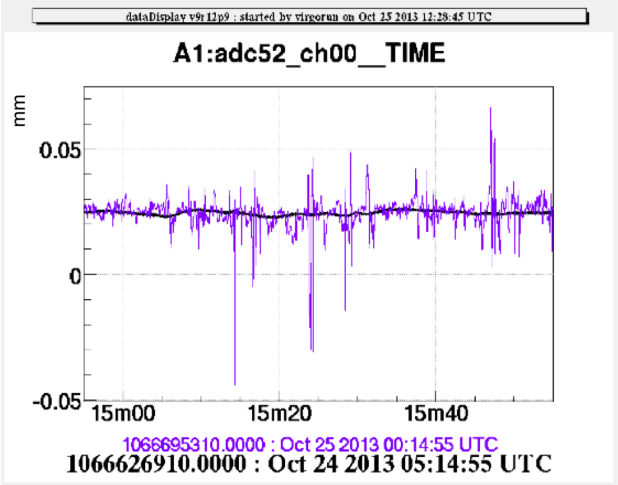

Figure 27: Near Field quadrant short time (60 s) signal measured for a standard mount: comparison between the configuration with boxes and cover on the setup and configuration without protections.

optical levers, and the protection windows of the quadrant photodiodes. Beams reflected by the quadrant are dumped with diaphragms on the optical path. Beams back-reflected by the output window of the vacuum tank and by the beam-splitter are more critical since they can be reflected by the wall of the tank and recombined with the main optical beam. Therefore, the system is very sensitive to the alignment of the optical elements, in particular of the optics under test. Figure 28 show the spectrum measured with the same standard mount under test with two different alignments.

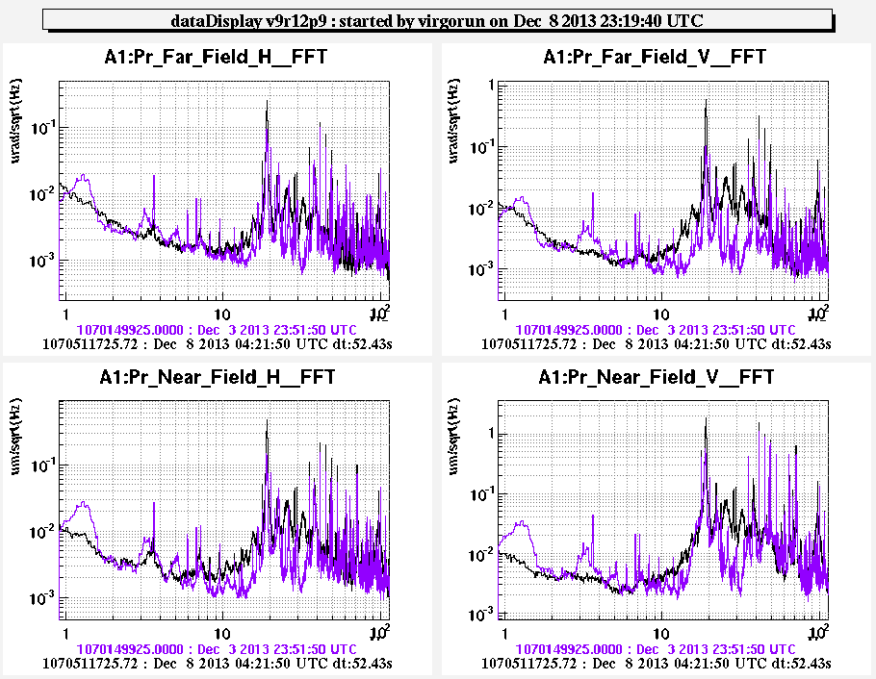

Figure 28: Spectra obtained in all degrees of freedom in two different alignment conditions of a standard mount: top (left) pitch (right) yaw, bottom (left) x (right) y.

The different level of the noise between 10 Hz and 50 Hz and the short time rms seem to be due to the scattered light. For this reason the comparison between the short time measurements of the optics under test and the setup is not representative. Moreover, the spectra on the figure 28 cannot be exploited to conclude on the resonance frequencies of the mounts, because they are limited by the setup noise. Transfer functions are needed to measure the resonance frequencies of the mounts, as done in section 4.3.

4.2.2 Stability of the optical levers system

In order to characterize the stability and the drifts of the experimental setup, long time measurements (8 to 10 hours) have been made, using the standard mount. Figure 29 shows the long time measured signal in the angular - pitch and yaw - and in the transversal - x and y - degrees of freedom.

Results on x, y, pitch and yaw drift are of the order of 5 μrad and 5 μm, probably limited by temperature drifts (the installation of temperature probes is in progress to improve the system) and laser beam pointing stability.

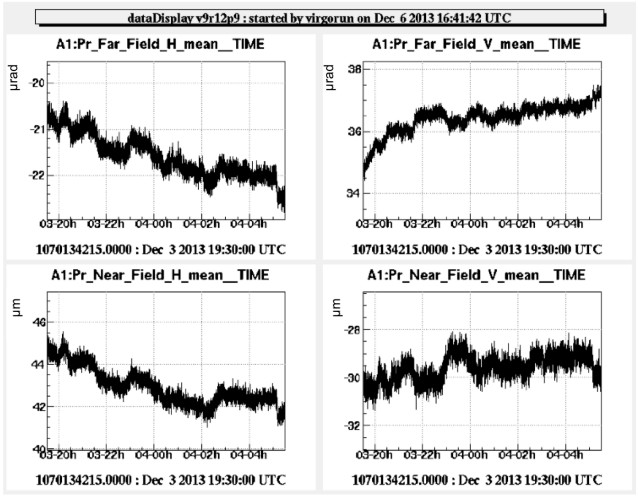

Figure 29: Typical signals of the experimental setup in the four degrees of freedom over 10 hours: top (left) equivalent yaw, (right) equivalent pitch; bottom (left) equivalent x, (right) equivalent y.

4.2.3 MMT_L mount

Figure 30 shows a comparison between long time (10 hours) measurements made respectively with the meniscus lens mount and a standard mount (purple curve) under test. It can be noticed that the drift induced by the meniscus lens mount and the rms are comparable with the ones of the setup. Then, no suspect drift are induced by the meniscus lens mount and the stability seems to be limited by the experimental conditions. Moreover, no suspect glitches are measured.

In conclusion, the stability of this mount have been studied. No suspect glitches (which could be responsible of a mechanical problem in the mount) have been highlighted. Moreover, the drift of the mount is compatible with the drift of the setup (4 μrad). The final mount will be placed on a suspended bench, under vacuum, with a control of the temperature better than 0.1 degree (not the case in our experiment) which can improve the stability of the mechanical mount. According to the table 4, during science mode the maximum tilt allowed for MMT_L is 1 mrad and the maximum shift is 100 μm. Previous results show that the MMT_L mount respect the specifications.

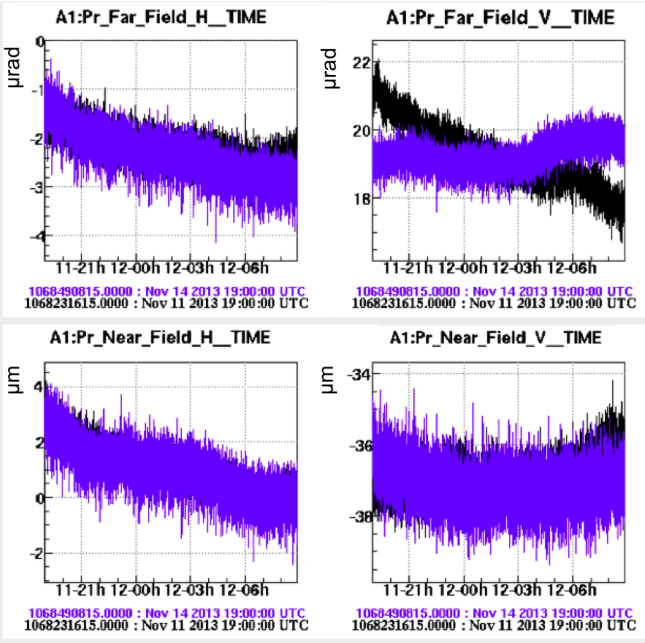

Figure 30: Ten hours measurement of the meniscus lens mount stability in the plane mirror configuration (black curve) compared to the stability of the setup (purple curve): top (left) yaw, (right) pitch; bottom (left) x, (right) y.

4.2.4 MMT_M1 mount

Figure 31 shows a comparison between long time (10 hours) measurements made respectively with M1 (black curve) and a standard mount (purple curve) under test. It can be noticed that the drift induced by M1 mount is comparable with the one of the setup (of the order of 2μrad and 4 μm).

In conclusion, the stability of this mount have been studied. No suspect glitches (which could be responsible of a mechanical problem in the mount) have been highlighted. Moreover, the drift of the mount is compatible with the drift of the setup (4 μrad). As for the meniscus lens, the final mount will be placed on a suspended bench, under vacuum, with a control of the temperature better than 0.1 degree (not the case in our experiment) and using a stabilized laser beam. All these improvements will allow to decrease the drift of the mount by a factor 3 or 4.

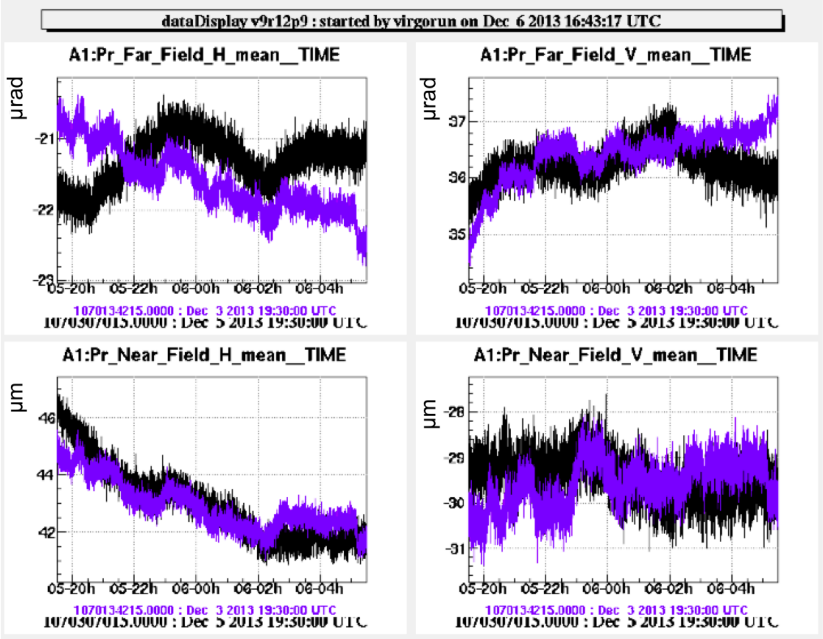

Figure 31: Ten hours measurement of the MMT_M1 mount stability (black curve) compared to the stability of the setup (purple curve): top (left) yaw, (right) pitch; bottom (left) x, (right) y.

4.2.5 MMT_M2 mount

Figure 32 shows a comparison between long time (12 hours) measurements made respectively with M2 (black curve) and a standard mount (purple curve) under test. The drift of the M2 mount is compatible with the drift of the setup which mean that we are also limited by the experimental conditions.

In conclusion, the stability of this mount have been studied. No suspect glitches (which could be responsible of a mechanical problem in the mount) have been highlighted and the drift of the mount is compatible with the drift of the setup (4 μrad). According to the table 4, during science mode the maximum tilt allowed for M2 is 6.8 μrad and the maximum shift is 10 μm. The previous results show that the M2 mount respect the specifications.

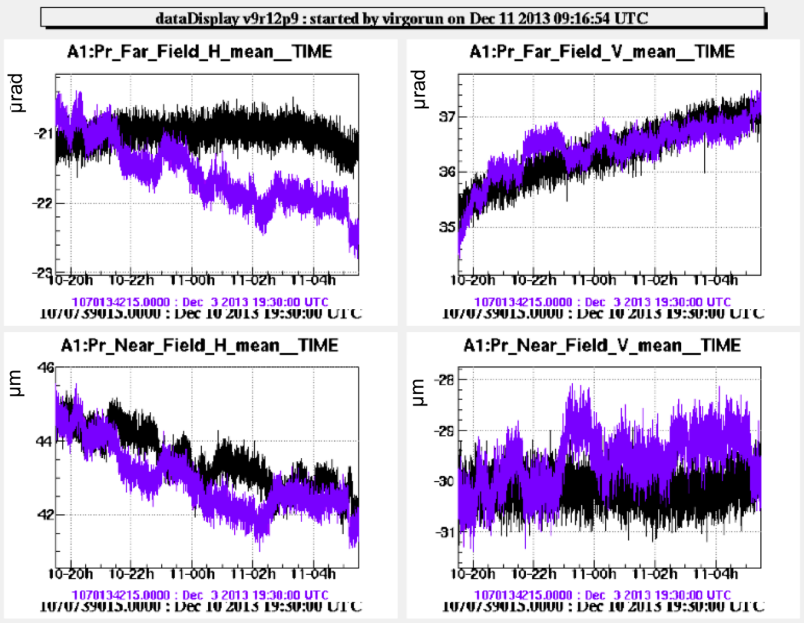

Figure 32: Twelve hours measurement of the MMT_M2 mount stability (black curve) compared to the stability of the setup (purple curve): top (left) yaw, (right) pitch; bottom (left) x, (right) y.

4.3 Vibrational Study

The resonance frequencies and the quality factors of the telescope mounts are measured for two reasons:

- to make a catalog of the resonance frequencies useful during the commissioning for peak identification
- to evaluate the impact of the scattered light

In the tests, an electromagnetic actuator is used for the excitation of the mounts. The transfer function between the quadrant signals, which depends on the movement of the mounts, and the voltage applied to the coil has been measured[4]. These tests have been made in air and under vacuum. In order to measure resonance frequencies and to estimate their quality factors, a simple theoretical model, which fit the obtained curves, has been implemented.

4.3.1 MMT_L Mount

In all the tests, a swept sine signal has been sent to the coil. The coherence has been measured in order to better understand frequency ranges in which applied force has induced a true motion on the mount: only the results obtained at frequencies with a high level of coherence have been considered. Figure 33 shows the measured coherence for pitch and yaw in air and under vacuum (residual pressure $p = 4.5 * 10^{-5}$ mbar).

Moreover, transfer functions have been measured in different vacuum conditions, in order to understand if the amplitude of the resonance peaks could vary in function of the residual pressure. Figure 34 shows a zoom in the frequency range of the resonance peaks of the transfer functions measured in different conditions (air, vacuum $p = 3.4 * 10^{-4}$ mbar and vacuum $p = 4.5 * 10^{-5}$ mbar, respectively in pitch and yaw).

[4]Tapping tests using an accelerometer were initially used but with results of lower quality and without the possibility to go under vacuum.

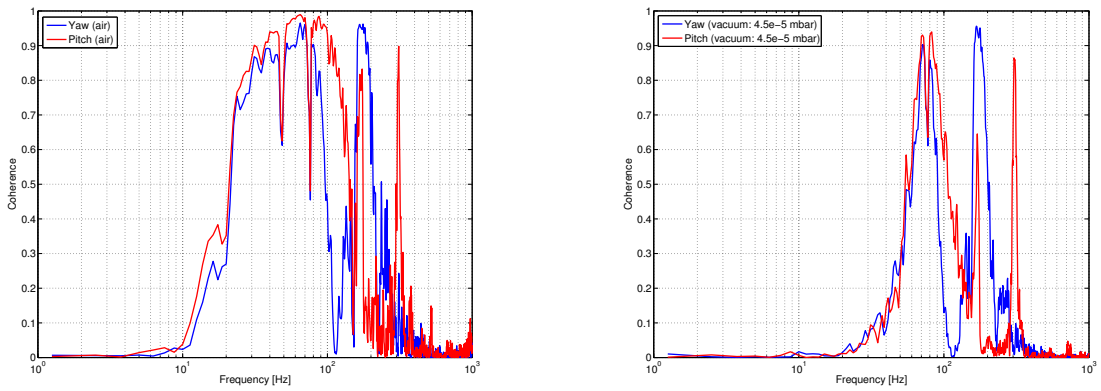

Figure 33: Meniscus lens mount: coherence measured in air (left) and under vacuum (right).

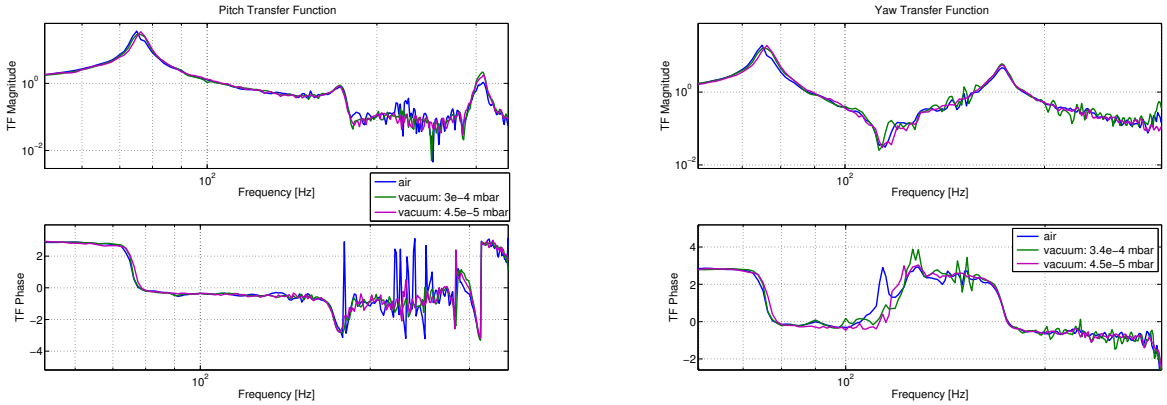

Figure 34: Meniscus lens mount: measured transfer functions in different vacuum conditions respectively in pitch (left) and yaw (right).

The same results have been obtained in different experimental conditions (in air and under vacuum) for what concerns both the frequency and the amplitude of the different peaks.

To evaluate the resonance frequencies and their quality factors, the transfer functions have been compared with a simple model, which is the sum of three harmonic oscillators and can be described as:

$$F(\omega) = A_1 \frac{\omega_1^2}{\omega_1^2 - \omega^2 + j\omega\frac{\omega_1}{Q_1}} + A_2 \frac{\omega_2^2}{\omega_2^2 - \omega^2 + j\omega\frac{\omega_2}{Q_2}} + A_3 \frac{\omega_3^2}{\omega_3^2 - \omega^2 + j\omega\frac{\omega_3}{Q_3}} \tag{4.4}$$

where A_1, A_2 and A_3 are three coupling coefficients, $f_1 = \omega_1/2\pi$, $f_2 = \omega_2/2\pi$ and $f_3 = \omega_3/2\pi$ are the frequencies of the resonance peaks and Q_1, Q_2 and Q_3 are their quality factors.

The parameters used in the simple model in order to adjust the transfer function measured for pitch are the following:

- $f_1 = 75$ Hz, $f_2 = 172$ Hz, $f_3 = 305$ Hz
- $Q_1 = 40$, $Q_2 = 20$, $Q_3 = 40$
- $A_1 = 1$, $A_2 = -0.03$, $A_3 = 0.02$

A comparison between the measured transfer function and the model is shown in figure 35.

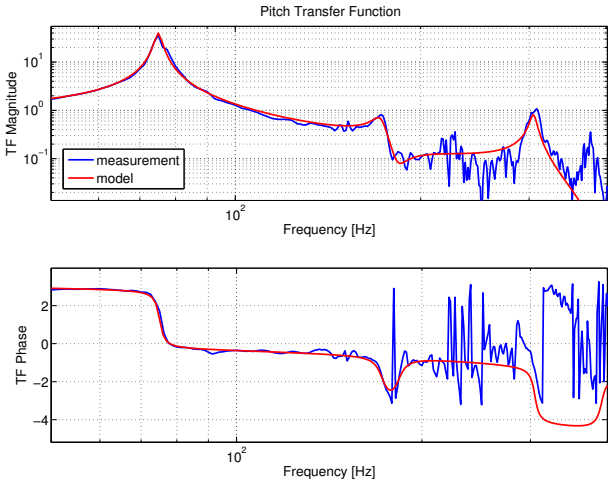

Figure 35: Meniscus lens mount: comparison between measured transfer function and simple model for pitch.

In the estimation of the values of the quality factors, a precision of a factor 2 is enough to understand the behavior of the mount in the amplification of the scattered light noise. In order to validate the accuracy of the model, measured transfer functions have been fitted with the same model, varying the parameters. As an example, figure 36 shows the main resonance frequency measured for pitch fitted with the same model but different values of the quality factor Q; Qs equal to 20, 40 and 60 have been used. It can be noticed that the best comparison is obtained for Q = 40 and, for the other values, the amplitude of the peak of the resonance frequency is not well fitted, confirming the validity of the adopted model.

The parameters used in the simple model in order to fit the transfer function measured for yaw are the following (the third resonance frequency is not considered since the level of the coherence is very low around 300 Hz):

- $f_1 = 75$ Hz, $f_2 = 172$ Hz
- $Q_1 = 40$, $Q_2 = 20$
- $A_1 = 0.65$, $A_2 = 0.3$

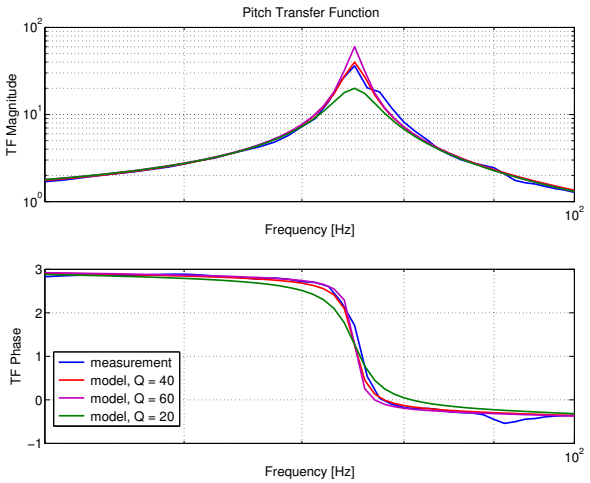

Figure 36: Meniscus lens mount: comparison between measured transfer function and simple model for pitch with different values of the quality factor.

A comparison between the measured transfer function and the model is shown in figure 37.

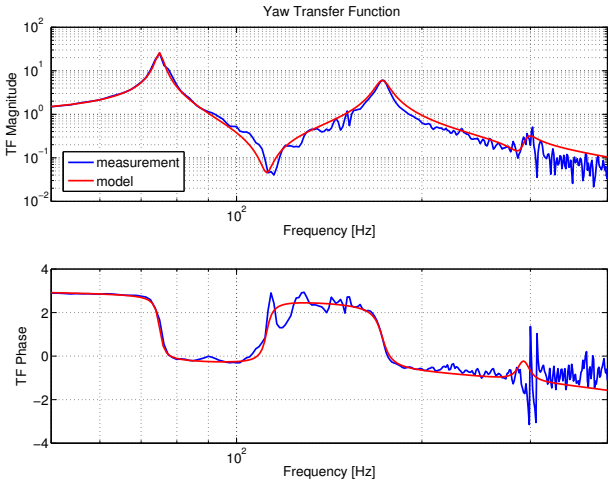

Figure 37: Meniscus lens mount: comparison between measured transfer function and theoretical model for yaw.

4.3.2 MMT_M1 Mount

The induced motion of the mount has been measured in the two angular degrees of freedom, pitch and yaw, using the Far Field quadrant. In all the tests, also the coherence has been measured in order to better understand frequency ranges in which applied force has induced a true motion on the mount: only the results obtained at frequencies with a high level of coherence have been considered. Figure 38 shows the measured coherence for pitch and yaw in air and under vacuum (residual pressure $p = 1.9 * 10^{-4}$ mbar).

Moreover, transfer functions have been measured in different vacuum conditions, in order to understand if the amplitude of the resonance peaks could vary in function of the residual pressure. Figure 39 shows a zoom in the

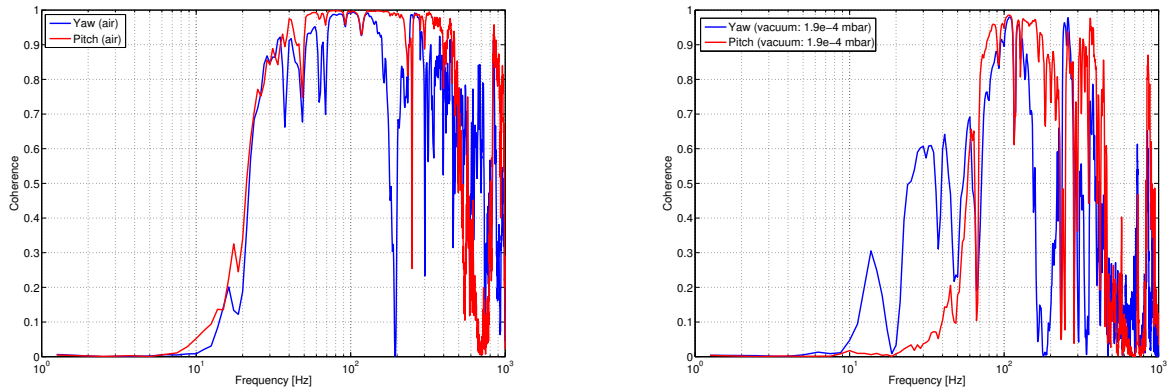

Figure 38: Parabolic mirror M1 mount: coherence measured in air (left) and in vacuum (right).

frequency range of the resonance peaks of the transfer functions measured in different conditions (air, vacuum $p = 1.9 * 10^{-4}$ mbar and vacuum $p = 4 * 10^{-5}$ mbar, respectively in pitch and yaw).

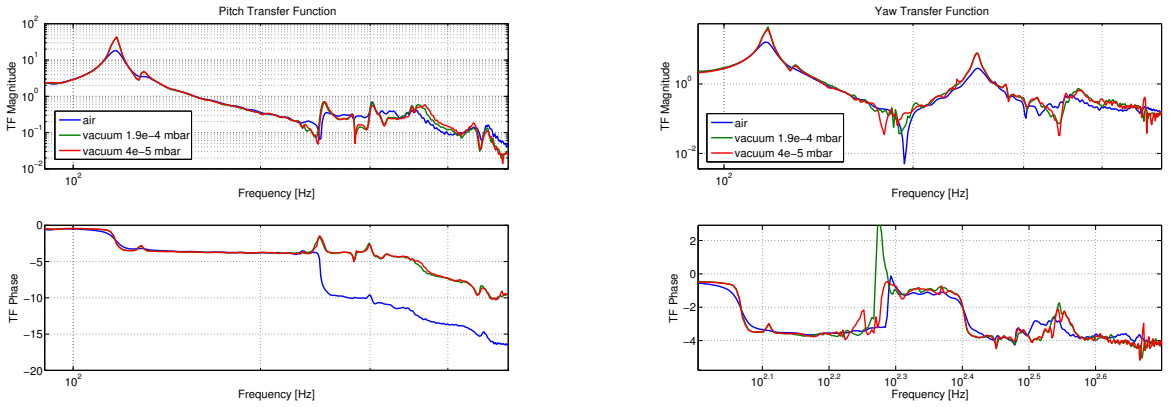

Figure 39: Parabolic mirror M1 mount: measured transfer functions in different vacuum conditions respectively for pitch (left) and yaw (right).

Figure 39 shows that the same resonance frequencies have been measured in air and under vacuum but the amplitude of the peak measured in air is lower than the ones measured in vacuum. Moreover, it can be noticed that the amplitude obtained in the two tests performed in vacuum is the same.

In order to better understand the behavior of the mount, in particular in order to measure resonance frequencies, to estimate their quality factors and to understand the difference between the results in air and under vacuum, the measured transfer functions have been compared with the same theoretical model described in equation 4.4.

The parameters used in the theoretical model in order to fit the transfer function measured for pitch in air are the following:

- $f_1 = 116$ Hz, $f_2 = 252$ Hz, $f_3 = 357$ Hz
- $Q_1 = 20$, $Q_2 = 20$, $Q_3 = 20$
- $A_1 = 0.9$, $A_2 = 0.009$, $A_3 = -0.02$

A comparison between the transfer function measured in air and the model is shown in figure 40.

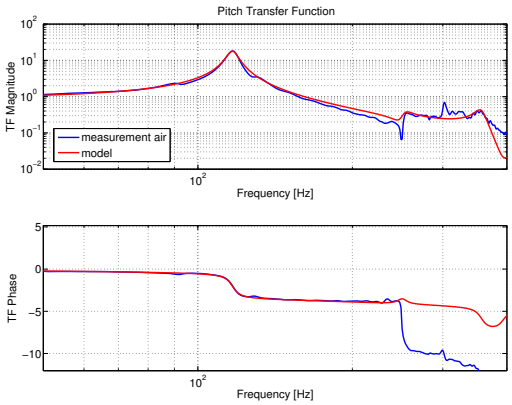

Figure 40: Parabolic mirror M1 mount: comparison between measured transfer function and simple model for pitch (air condition).

The parameters used in the theoretical model in order to fit the transfer function measured for pitch in vacuum are the following:

- $f_1 = 116$ Hz, $f_2 = 252$ Hz, $f_3 = 365$ Hz
- $Q_1 = 40$, $Q_2 = 40$, $Q_3 = 20$
- $A_1 = 0.9$, $A_2 = 0.02$, $A_3 = -0.02$

A comparison between the transfer function measured in vacuum and the model is shown in figure 41.

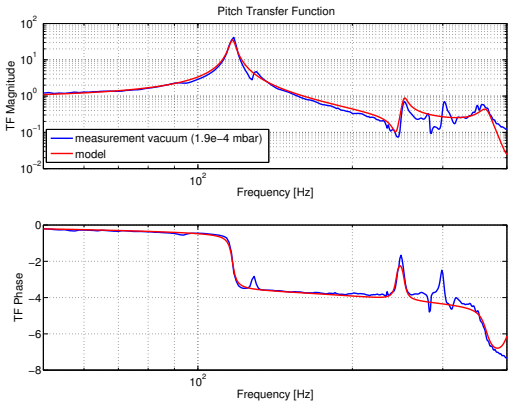

Figure 41: Parabolic mirror M1 mount: comparison between measured transfer function and theoretical model for pitch (vacuum condition).

It can be noticed that resonance frequencies are the same in air and under vacuum condition, while estimated quality factors are different. In particular, considering the first main frequency, the value of the quality factor measured under vacuum is double with respect the one measured in air.

The parameters used in the theoretical model in order to fit the transfer function measured for yaw in air are the following:

- $f_1 = 116$ Hz, $f_2 = 252$ Hz, $f_3 = 355$ Hz
- $Q_1 = 20$, $Q_2 = 20$, $Q_3 = 20$

- $A_1 = 0.76$, $A_2 = 0.15$, $A_3 = 0.03$

A comparison between the transfer function measured in air and the model is shown in figure 42.

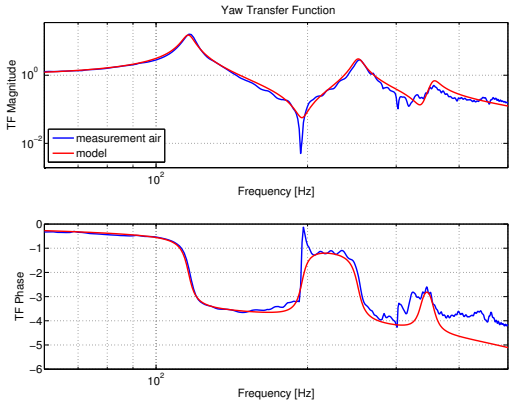

Figure 42: Parabolic mirror M1 mount: comparison between measured transfer function and simple model for yaw (air condition).

The parameters used in the theoretical model in order to fit the transfer function measured for yaw in vacuum are the following:

- $f_1 = 116$ Hz, $f_2 = 252$ Hz, $f_3 = 365$ Hz
- $Q_1 = 40$, $Q_2 = 40$, $Q_3 = 20$
- $A_1 = 0.85$, $A_2 = 0.2$, $A_3 = 0.006$

A comparison between the transfer function measured in vacuum for yaw and the model is shown in figure 43.

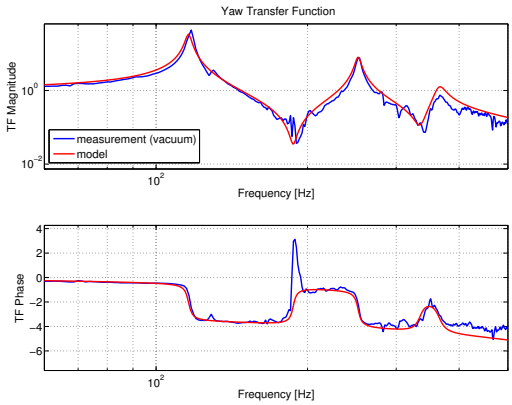

Figure 43: Parabolic mirror M1 mount: comparison between measured transfer function and theoretical model for yaw (vacuum condition).

Also for the yaw degree of freedom, resonance frequencies are the same in air and in vacuum conditions. The estimated quality factors are different with the values measured in vacuum that is double with respect to the one measure in air. Since mounts will be used in vacuum, in the following only quality factors estimated in vacuum will be considered.

4.3.3 MMT_M2 Mount

The induced motion of the mount has been measured in the two angular degrees of freedom, pitch and yaw, using the Far Field quadrant. The experimental setup used for the tests on M2 was the more critic to implement: in fact, the radius of the coil was a bit larger than the one of the mirror mount, therefore the available room to induce the excitation was a bit small. The magnet has been glued not in the center of the fake mirror and some coupling could be present in the experimental results. In all the tests, also the coherence has been measured in order to better understand frequency ranges in which applied force has induced a true motion on the mount: only the results obtained at frequencies with a high level of coherence have been considered. Figure 44 shows the measured coherence for pitch and yaw in air and in vacuum (residual pressure $p = 1.6 * 10^{-4}$ mbar) conditions.

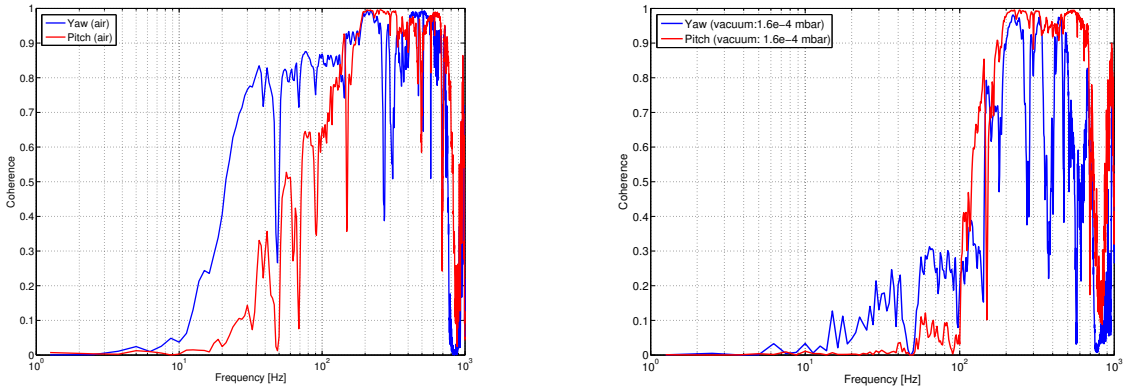

Figure 44: Parabolic mirror M2 mount: coherence measured in air (left) and in vacuum (right) conditions.

A comparison between the measured transfer functions in air and under vacuum for pitch and yaw is shown in figure 45.

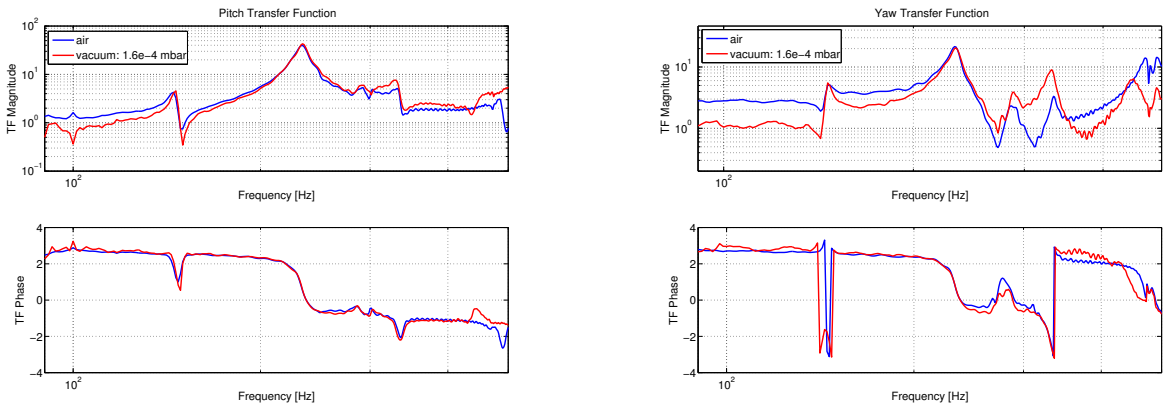

Figure 45: Parabolic mirror M2 mount: measured transfer functions in different conditions respectively for pitch (left) and yaw (right).

It can be noticed that the first and the second resonance frequencies and their amplitude are the same in air and in vacuum. In yaw degrees of freedom measurements in air and in vacuum are slightly different for what concerns both the flat part at low frequencies and the higher resonance peaks. Since measurements were a bit noisy and the coherence was not very good in all the spectrum, the two first resonance peaks have been chosen as reference. In order to better understand the behavior of the mount, in particular in order to measure the

resonance frequencies and to estimate their quality factors, measured transfer functions have been compared with the same theoretical model described in equation 4.4.

The parameters used in the theoretical model in order to fit the transfer function measured for pitch under vacuum are the following:

- $f_1 = 145$ Hz, $f_2 = 232$ Hz, $f_3 = 331$ Hz
- $Q_1 = 20$, $Q_2 = 30$, $Q_3 = 30$
- $A_1 = 0.14$, $A_2 = 1.36$, $A_3 = -0.1$

A comparison between the transfer function measured in vacuum and the model is shown in figure 46.

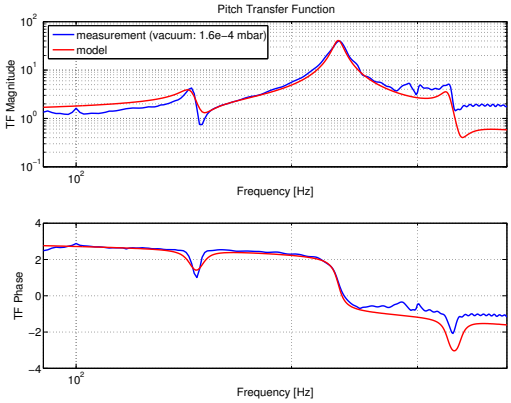

Figure 46: Parabolic mirror M2 mount: comparison between measured transfer function and theoretical model for pitch (vacuum condition).

The parameters used in the theoretical model in order to fit the transfer function measured for yaw under vacuum are the following (also the fourth resonance frequency is considered since its amplitude is higher than the third in the measurement):

- $f_1 = 116$ Hz, $f_2 = 232$ Hz, $f_3 = 288$ Hz, $f_4 = 331$ Hz
- $Q_1 = 40$, $Q_2 = 20$, $Q_3 = 30$, $Q_4 = 50$
- $A_1 = -0.15$, $A_2 = 0.9$, $A_3 = 0.1$, $A_4 = -0.2$

A comparison between the transfer function measured under vacuum for yaw and the model is shown in figure 47.

It can be noticed that the main resonance frequency is at 232 Hz, with a quality factor that is slightly different in pitch and yaw, respectively 30 and 20.

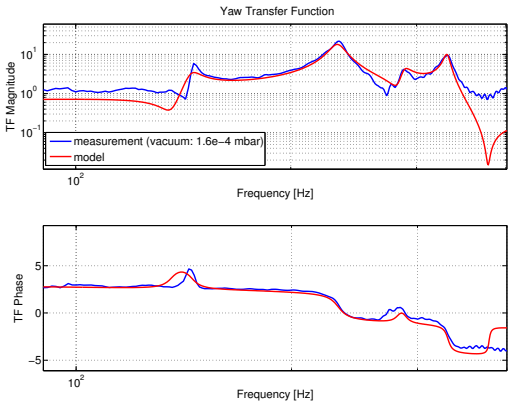

Figure 47: Parabolic mirror M2 mount: comparison between measured transfer function and theoretical model in yaw (vacuum condition).

4.3.4 Summary of the MMT resonance frequencies

In tables 13 and 14 a summary of the resonance frequencies measured in vacuum, respectively for pitch and yaw, for all the Mode Matching Telescope mounts is shown.

	Meniscus Lens	**Parabolic Mirror M1**	**Parabolic Mirror M2**
Frequency 1 (Hz)	75	116	145
Q	40	40	20
Frequency 2 (Hz)	172	252	232
Q	20	40	30
Frequency 3 (Hz)	305	365	331
Q	40	20	30

Table 13: MMT mounts resonance frequencies measured for pitch.

	Meniscus Lens	**Parabolic Mirror M1**	**Parabolic Mirror M2**
Frequency 1 (Hz)	75	116	116
Q	40	40	40
Frequency 2 (Hz)	172	252	232
Q	20	40	20
Frequency 3 (Hz)	-	365	288
Q	-	20	30
Frequency 4 (Hz)	-	-	331
Q	-	-	50

Table 14: MMT mounts resonance frequencies measured for yaw.

The initial design of the mounts included resonance frequencies higher than 100 Hz, also for the meniscus lens. The discrepancy between simulations and experimental measurements can be explained by the lack of the picomotors and the approximation of the stiffness of the rails in the mechanical model. Since the MMT_M2 and the meniscus lens are very close, it was not possible to modify the design of the second one by introducing rails on both sides in order to increase its rigidity. Anyway, a clamp on the ”free” side (the one without rails) can be added if necessary.

5 Diffused Light Noise

In order to calculate contributions to the scattered light noise of the mounts we multiply the noise projection shown in figure 2 by the quality factor for each resonance frequency. We remark that the level of the scattered light noise always remains below h/2000. This estimation is even more conservative for MMT_M1 and MMT_M2 since curve in figure 2 is computed for the meniscus lens, which is the most critical element. Therefore, it can be concluded that the mechanical mounts of the mode matching telescope are not a limiting factor for the scattered light noise.

6 Conclusions

- The calibration factors between radians and steps of the picomotors and between meters and steps of the picomotors have been measured for all the mounts. They are in agreement with the expected values.
- The system made of picomotors, rails and springs works properly in vacuum for the three mounts.
- Upper limits of the coupling between rotations and translations have been found and are of the order of 5 %.
- No strange glitches have been observed with all the mounts under test.
- Upper limits on the drifts of the mounts are of the order of 5 μrad and 5 μm over 10 hours (drifts of the optical levers system used for the measurements).
- Resonance frequencies have been measured for all the mounts in vacuum. They are in a range between 75 Hz and 400 Hz. Quality factors measured in vacuum are between 20 and 50.
- Considering all the measured resonance frequencies and quality factors, the diffused light noise projection remains below h/2000.

A Appendix A - Modification of the gimbal mounts of the parabolic telescopes

A.1 History of the gimbal mounts

Mechanical mounts of the parabolic mirrors (MMT_M1 and MMT_M2) of the injection and dark fringe telescopes are made with a gimbal system. This design implies that the mounts are, in principle, more stable and rigid than cinematic mounts and the rotation point is placed on the center of the optics.

The gimbal axes have been realized according to the scheme below (figure 48):

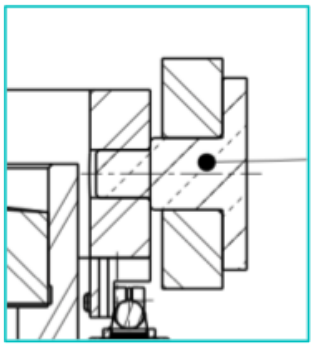

Figure 48: First design of the gimbal axes for the MMT_M1 and MMT_M2 mechanical mounts.

The gimbal axes were cylindrical and fitted together in the mirror mount by a cylindrical hole. The dimensions of the axis were ϕ8H7 and dimensions of the hole in the mirror mount was ϕ8g6. This means that the minimum clearance of the axes is 5 μm and the maximum clearance is 29 μm, allowing the rotation of the axis.

During the tests of the MMT_M1 mount at APC, we found a backlash on the vertical gimbal axis of the order of 20 μm. This backlash could introduce some uncontrolled motions on the mount above the specifications (see Table 4). We studied then an alternative solution: a gimbal axis with a ball, as shown in the scheme below (figure 49):

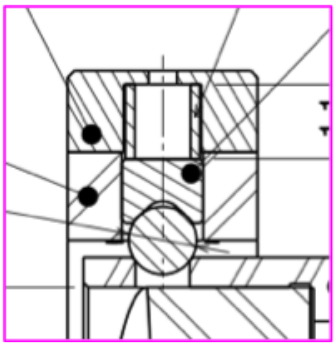

Figure 49: Second design of the gimbal axis for the MMT_M1 and MMT_M2 mechanical mounts.

A ceramic ball, held by a spring, is in contact with the mirror mount, allowing a smooth rotation with a single point of contact between the ball and the mirror mount. No backlash is possible using this system and the spring maintains the position of the ball. Careful thoughts and discussions about the integration of this system on all the gimbal axes (horizontal and vertical) or only on the axis where the problem was detected (vertical axis) have been made. On the horizontal axis, even if a backlash of a few microns is present, in principle it should not generate a displacement of the mount, since the weight of the mount keeps the gimbal axis always in contact with the mirror holder. In addition, the mounts have been extensively tested under vacuum at APC, and no problems have been detected on the horizontal axis. To fit the schedule and avoid any additional changes on a mount that works, we decided to change only the vertical axis.

A.2 Re-Assembly of the mounts at Cascina: after cleaning

Mechanical mounts have been dismounted at APC, packaged and sent to EGO. During the re-assembly phase of mechanical mounts, we realized that it was very difficult to introduce the horizontal gimbal axis in the mount and impossible to rotate MMT_M2 around the horizontal axis of rotation. MMT_M1 mount could be assembly without difficulty, but the horizontal rotation was also difficult.

A.3 Assumptions

- Explanation 1: thermal expansion

A first assumption is that the materials were inflated due to temperature differences, and were therefore difficult to fit and move. The thermal expansion of these materials is of the order of:

δL = α x L x δT

where α is the thermal expansion coefficient, L the length of the material and δT temperature difference.

For aluminum: δL = 23.1 x 10^{-6} x 10 x 10^{-3} x 5 = 1.1 μm

For bronze: δL = 17.5 x 10^{-6} x 10 x 10^{-3} x 5 = 0.87 μm

Since there are less than 5 degrees of difference between the APC clean room and the EGO clean room, this hypothesis seems unrealistic.

- Explanation 2: oxidation

An oxide layer has been grew after cleaning mechanical parts, when they have been in contact with air. This oxide layer could increase the diameter of the gimbal axis of bronze (or decrease the diameter of the holes in aluminum), and thus lead to a difficult assembly and a rotation impossible. Natural oxide layer (at least for bronze) is about 50 Angstrom, too small with respect to the clearance of the hole.

- Explanation 3: removal of oxide during the cleaning

It is possible that an oxide layer was present on the mounts (including gimbal axis) in our tests at APC (as well as some residual machining lubricant). Oxide layers reduce friction and so our rotational tests proceed without any issue. After cleaning the parts at EGO, this oxide layer (and any other deposits on the mounts) have been removed. Both materials (bronze and aluminum) were in dry contact and the parts may even seize. This has lead to difficulties in introducing the gimbal axis and also to move the mechanical mounts.

A.4 Tests

Vacuum grease (lubricant that enhance friction) was placed on the gimbal axis of M1. This allowed to move again perfectly the mount. Then the mount was placed under vacuum. After 2 days of testing, the mount was still moving perfectly and there were no problem of outgassing. The vacuum grease has a very good thermal

stability (-40 degrees to 200 degrees) and thus a long-term constant properties. This test confirms that the explanation 1 or 2 are not valid. The thickness of the layer of vacuum grease that was placed on the gimbal axis is much larger than the thickness of the natural oxide film or the thermal expansion of the materials. If the oxide layer (or expansion) had prevented a horizontal rotation, the deposit of vacuum grease would not have improved the behavior of the mounts.

A.5 Conclusions et proposed solutions

The assumption 3 - removing an oxide layer - is the most convincing one. This has caused the seize between the two materials (aluminum and bronze). The use of two different materials at the gimbal axis seems to be the best solution, but the association aluminum-bronze is probably not perfect. We have to improve the friction at this level.

MMT_M2 mount can be modified with horizontal axis with balls (like the vertical one) as shown in figure 50. No changes are expected on the mirror mount, the balls are already in stock, the springs are already in stock, and we just have to update the mechanical plans and subcontract the parts. All this has been studied and sent to subcontracting in 2 days. Parts will arrive at the APC before February 5, 2014, the mount can be tested and send to EGO before 11 February,2014 for a planned implementation on 13/14 February, 2014 and an alignment of the telescope during the week of February 17, 2014.

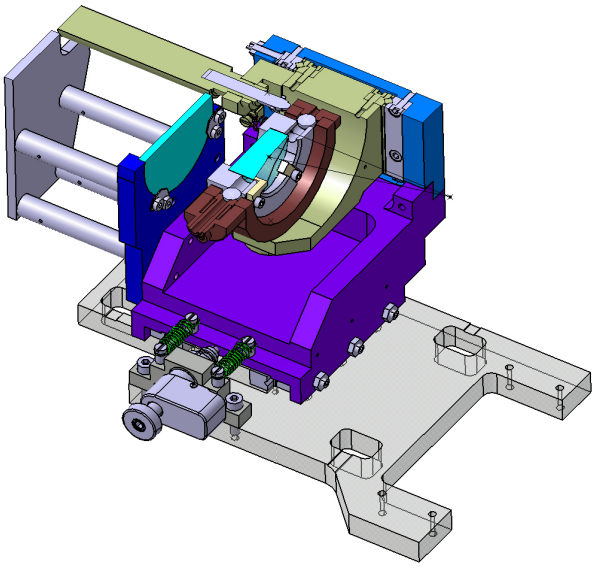

Figure 50: New CAO design of the MMT_M2 mount including the horizontal gimbal axis with balls.

For the MMT_M1 mount it is more complicated because we have strong space constraints. As shown in figure 51, a laser beam passes close to the right of the mount, and an other mirror mount is situated very close to the left. The preliminary study was done: we can put gimbal axis with balls within these space constraints but we have to modify the gimbal ring and subcontract 5 additional parts. Modifications on the gimbal ring can be critical (figure 52), we take the risk to damage the part and modify all its features. Furthermore, there may be torsion problems on the gimbal axis due to the weight of the mirror (M1 is much heavier than M2), which may offset the gimbal axis and prevent rotation. The study of horizontal axis with balls on MMT_M1 mount must take more time and we are not sure on an optimal result.

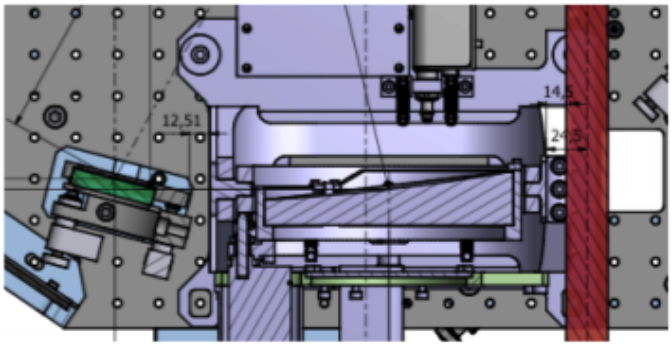

Figure 51: Space constraints around MMT_M1 mount.

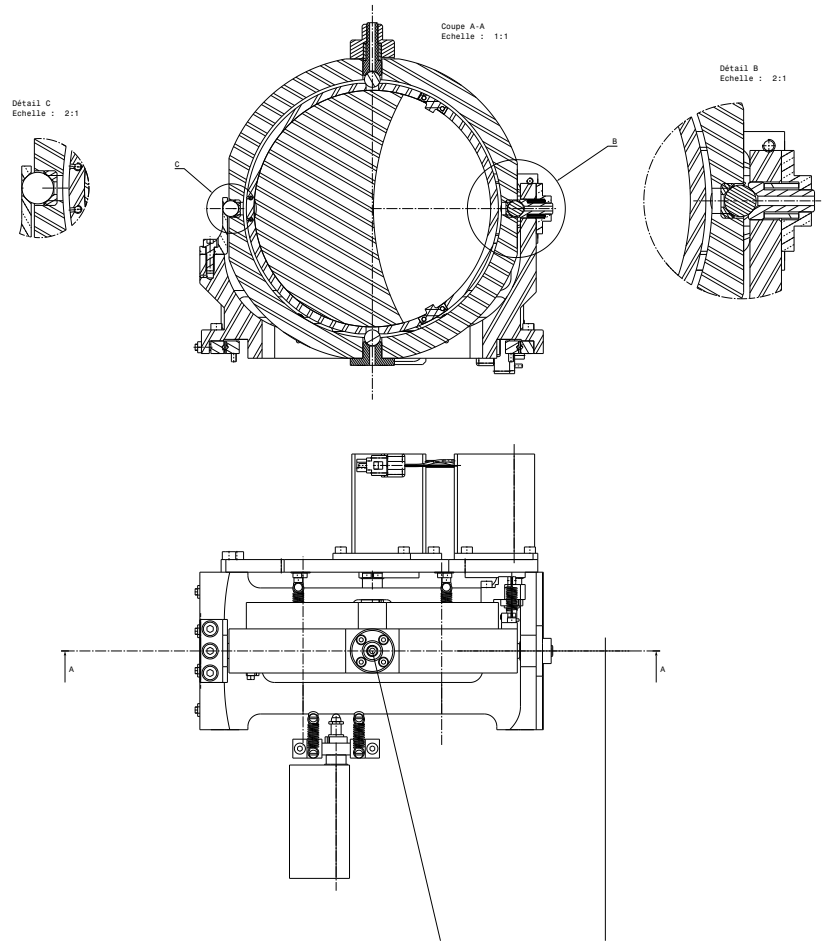

Figure 52: Possible design for the MMT_M1 mount including horizontal gimbal axis with balls.

We know that vacuum grease solves the problem (and also allows us to give an explanation to the problem). The conclusion is that it is better to leave this mount as it is (it works and we will not take the risk of dramatically shift the schedule). Vacuum grease is long-term thermally stable and should not prevent the rotation of the axis even if we move the mount in few months. However, to anticipate any problem, we could move the mount once a month since this axis is controlled by closed loop picomotors. We can operate a hundred steps on the picomotor, we go back to the original position and so maintain the initial position of the mirror while allowing

good homogeneity of vacuum grease on the horizontal gimbal axis.

In addition, a gimbal axis with a dry lubricant coating (i.e DLC) could be used as back-up solution for injection if we ever meet a problem with vacuum grease.

Moreover, this friction problem is not encountered on the axis with balls since these ones are in ceramic, a very hard and smooth material. However, when we have re-assembled the mounts, we saw that on the bottom vertical axis (which is aluminum), a slight layer of aluminum was deposited on the ceramic ball. On the top gimbal axis (which is bronze), there was nothing. Aluminum is a softer material than bronze, and could be damaged through a strong friction process. As a precautionary measure, we changed the material of bottom vertical axis of the two mounts (MMT_M1 and MMT_M2) choosing bronze.

A.6 Solutions for the dark fringe telescope

For the dark fringe telescope, we will use axis with balls for both horizontal and vertical of MMT_M1 and-MMT_M2 since the space constraints on the detection bench SDB1 are less stringent than the injection bench SIB1 around the MMT_M1 mount.

References

[1] M. Barsuglia et al., *"AdV INJ: Mode matching telescope configuration choice for the ITF input telescope"*, Virgo internal document VIR-0010B-12 (2012). 2, 3

[2] Virgo Collaboration, *"Advanced Virgo Technical Design Report"*, Virgo internal document VIR-0128A-12 (2012). 2

[3] P. Puppo , P. Rapagnani, *"The Electromagnetic Actuators of the Mirror Reaction Masses"*, Virgo internal document VIR-016A-09 (2009).

[4] M. Barsuglia et al., *"Backscattering from Advanced Virgo telescopes"*, Virgo internal document VIR-0211A-12 (2012).

[5] B. Canuel et al., *"Displacement noise from back scattering and specular reflection of input optics in advanced gravitational wave detectors"*, Optics Express, Vol. 21, No. 9, (2013).

[6] Personal communication by Eric Genin. 4